Time and energy calibration of large-volume segmented sodium-iodide detectors

Author:
Markus Preston

Supervisor:
Dr. Kevin Fissum

September 5, 2012

LUNDS UNIVERSITET
Naturvetenskapliga fakulteten

Abstract

Nuclear physics research is focused upon determining the structure of the atomic nucleus and nuclei, and understanding the interactions both within it and between them.

To accomplish this, various probes of the nucleus are used - two types are 'electromagnetic' and 'hadronic'. An example of an electromagnetic probe is the photon, which has the advantage of interacting with the nucleus via the very well-understood electromagnetic force.

At MAX-lab, tagged photons are produced using an electron beam. In order to detect these photons, different detectors may be used: sodium iodide and Pb-glass are two examples. In order to produce meaningful results, such detectors must first be calibrated by applying physically well-motivated and understood corrections. The detectors have to be calibrated both relatively and absolutely in terms of their timing and the amount of deposited energy they register. A detailed overview of such calibrations is presented in this thesis, which is based upon data acquired at MAX-lab during the June and September 2011 and April 2012 run periods.

Populärvetenskaplig sammanfattning

MAX-lab i Lund är den nationella elektronacceleratoranläggningen i Sverige. Elektronerna, som accelereras upp till hastigheter nära ljusets, används i forskning inom många olika områden. Ett av dessa är produktion av högenergetiska fotoner ("ljuspartiklar"). Dessa används i sin tur för att undersöka atomkärnan. Detta kan göras på flera olika sätt. Gemensamt för alla sätt är att det krävs detektorer för att detektera de partiklar som resulterar av reaktionen mellan fotonen och atomkärnan. Dessa detektorer måste kalibreras för att ge användbara svar.

Fotonerna som används i kärnfysikforskningen på MAX-lab produceras genom att låta elektronstrålen träffa en metallplatta, i vilken elektronerna bromsas upp. Då de bromsas upp förlorar de en del av sin energi, samtidigt som en foton med en energi motsvarande elektronens förlorade energi sänds ut. Fotonens energi kan bestämmas genom att jämföra elektronens energi före och efter denna inbromsning. Elektronenergin efter inbromsning bestäms med hjälp av en detektor som är indelad i 64 delar (*kanaler*), placerade så att varje kanal motsvarar en viss elektronenergi.

En atomkärna kan reagera med en foton på flera olika sätt. Exempelvis kan fotonen "studsa" mot atomkärnan och förlora en del av sin energi. Om energin på fotonen efter denna kollision kan mätas, och tillräckligt många fotoner skickas mot atomkärnan, kan sannolikheten för att just denna typ av reaktion inträffar bestämmas.

På MAX-lab används tre stora fotondetektorer för att mäta denna energi. Var och en av dessa består av stora kristaller av (tallium-aktiverad) natriumjodid, arrangerade på olika sätt.

I varje detektor finns flera *fotomultiplikatorer*, som omvandlar ljus till elektriska signaler. Dessa signaler görs om till digitala signaler med hjälp av elektronisk utrustning. Denna är inte kalibrerad, vilket gör att en viss fotonenergi inte motsvaras av samma digitala signal för alla fotomultiplikatorer i detektorn. Detta gör att elektroniken måste kalibreras så att en viss fotonenergi motsvarar en viss digital signal för hela detektorn.

Utöver energikalibreringen av detektorerna, måste även en tidskalibrering utföras. Detta för att kunna bestämma skillnaden i tid mellan det att en elektron träffar elektrondetektorn och det att en foton träffar fotondetektorn. Detta görs genom att jämföra denna tidsskillnad för alla 64 kanaler på elektrondetektorn, och kalibrera dem till samma tid.

Acknowledgements

First and foremost, I would like to thank my supervisor, Dr. Kevin Fissum for his continuous help and advice during this project. I would also like to thank Dr. John Annand at the University of Glasgow for allowing me to take part in the experiments in April, and also the rest of the Glasgow group for being very helpful during the entire run period. I would also like to thank Dr. Luke Myers for help during the writing of this thesis.

Contents

List of Figures

List of Tables

List of Abbreviations

CW	Continuous wave
DAQ	Data acquisition
EGS	Electron Gamma Shower
FP	Focal plane
FWHM	Full width at half maximum
LINAC	Linear accelerator
MeV	Mega electron volt
NaI(Tl)	Sodium Iodide (Thallium activated)
Pb-glass	Lead glass
PMT	Photomultiplier tube
PSR	Pulse-stretcher ring
QDC	Charge-to-digital converter
TDC	Time-to-digital converter

Chapter 1

Experiment

1.1 MAX-lab

MAX-lab is the national electron accelerator laboratory located in Lund, Sweden. It is operated jointly by Lund University and the Swedish Research Council. The facility is currently used for three areas of research: accelerator physics, synchrotron radiation research, and photonuclear research.

MAX-lab consists of three storage rings for electrons - MAX I, MAX II, and MAX III. Electrons may be fed into all three rings using an injector. Only the MAX I storage ring is used in nuclear-physics research. An overview of the injector, MAX I storage ring, and nuclear physics end station are presented in this chapter.

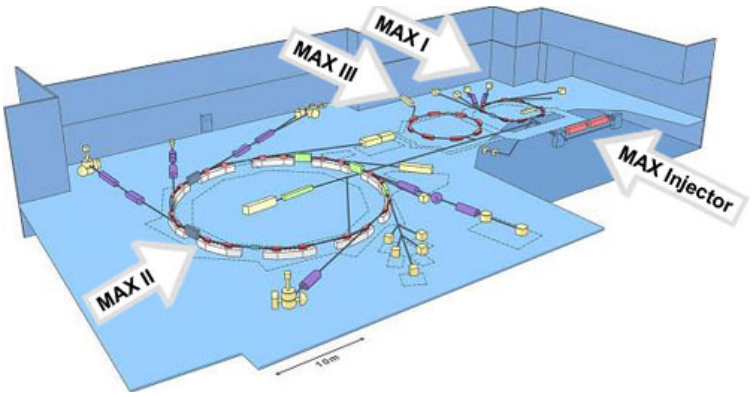

Figure 1.1: Overview of the MAX-lab facilities. Figure from Ref. [1].

1.2 The injector

The electrons used in all research at MAX-lab come from the injector. The injector consists of an electron gun and two linear accelerators (LINACs).

1.2.1 Electron gun

When a high voltage is applied across a cathode, the temperature of the cathode increases. When the temperature of the cathode reaches approximately 1000 °C, electrons are thermionically emitted from the filament. This is the procedure used to generate the electron beam. Once the electrons have escaped the cathode, they are accelerated up to energies of around 2 MeV by applying a strong electric field. For the purpose of photonuclear research, electrons are generated in pulses of length 200 ns, with the time between two pulses being 100 ms. Thus, the electron gun operates at a frequency of 10 Hz.

1.2.2 Linear accelerators

The 2 MeV electrons are collimated and fed into two consecutive LINACs. A LINAC works by accelerating charged particles using microwaves. Each LINAC at MAX-lab is able to accelerate electrons to nominal energies of 100 MeV. Since the injector consists of two consecutive LINACs, the electrons will have a nominal energy of 200 MeV when leaving.

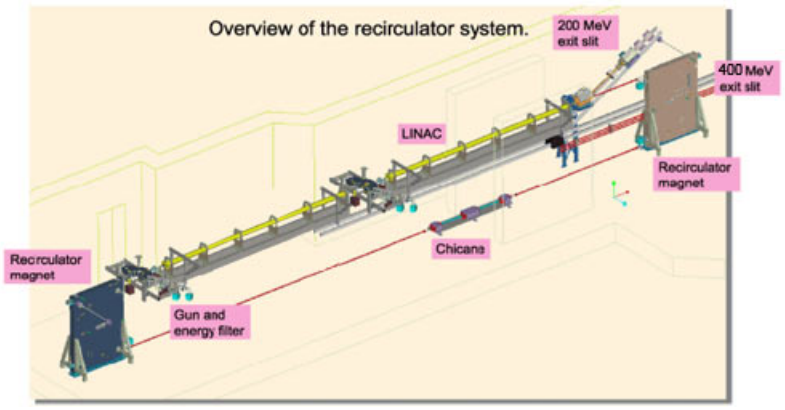

Figure 1.2: The MAX-lab injector. Seen in the figure is the electron gun, the two LINACs, and the exit slit. Figure from Ref. [2].

1.3 Electron storage ring

After an electron pulse has left the LINACs, it is injected into the MAX I pulse-stretcher ring (PSR). The purpose of a PSR is to stretch the injected electron pulse over time in order to produce as continuous a beam as possible. This is because the electronics and data-acquisition computers used in the experiments greatly prefer a continuous low-volume supply of data over intense short pulses of data which can overload the equipment and lead to all sorts of rate-dependent effects.

As previously mentioned, electron pulses enter the storage ring at a frequency of 10 Hz and with a pulse length of 200 ns. The MAX I ring has a circumference of 108 ns at the speed of the electrons, practically that of light. Thus, the electrons are injected over two roundtrips within the PSR. The pulses are then slowly extracted over the following 100 ms until the next pulse from the LINACs is injected, extending the duration of the injected pulse by a factor of 500 000. In this manner, a nearly countinuous beam (CW) is obtained.

1.4 Photon-beam production

1.4.1 Bremsstrahlung

The extracted CW electron beam is passed to the photonuclear area of MAX-lab. Bremsstrahlung photons are created by directing the beam onto a thin (approximately 100 μm) foil of aluminium (the radiator). A small fraction of the incident electrons produce bremsstrahlung photons. In this process, the energy of the incident beam electron is lowered, and a photon carrying the energy lost by the incident beam electron is produced. A typical distribution of the energies of the resulting bremsstrahlung photons is shown in Fig. 1.3.

1.4.2 Photon tagging

As mentioned above, the energy of the photons emitted via the bremsstrahlung process corresponds to the energy difference between the electron before and after the process, according to

$$E_\gamma = E_0 - E' \tag{1.1}$$

where
E_γ = energy of the bremsstrahlung photon
E_0 = energy of the electron before bremsstrahlung (the beam energy)
E' = energy of the electron after bremsstrahlung

Thus, if the energy of the electron beam is known, the energy of the resulting photon can be determined, provided that the energy of the corresponding post-bremsstrahlung electron can be measured. This is done by placing a dipole magnet close to the post-bremsstrahlung electron beam.

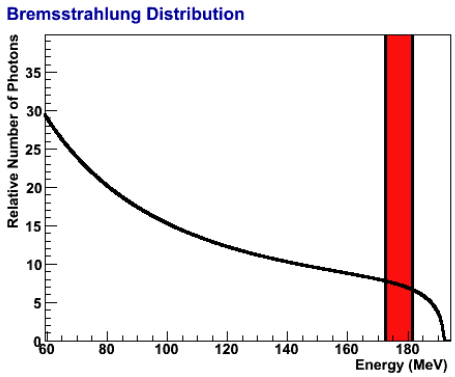

Figure 1.3: Bremsstrahlung photon-energy distribution. The maximum energy of the photons is the same as the electron beam energy - in this case 192.5 MeV. The red region is the energy range that can be examined due to the choice of magnetic field and placement of the focal-plane (see Sec. 1.4.2). It is adjustable. Figure from Ref. [3].

The Lorentz force is given by

$$\vec{F} = q_e(\vec{E} + \vec{v} \times \vec{B}) \tag{1.2}$$

where
$\vec{F}$ = Lorentz force
q_e = charge of the electron
$\vec{E}$ = applied electric field
$\vec{v}$ = velocity of the electron
$\vec{B}$ = applied magnetic field

Due to this force, the electrons bend away from their original path. The photons are unaffected because of their lack of electric charge. Since no electric field is present, the electrons will only be affected by the magnetic field.

As previously mentioned, the magnetic field is produced using a dipole magnet, which creates a field perpendicular to the electron path after the aluminium foil. This results in a curving of the electron path, as seen in Fig. 1.4.

Provided that the electron has undergone bremsstrahlung in the foil, it may have an energy sufficiently low for it to be bent onto the focal-plane (see Sec. 1.5) as shown in Fig. 1.4. The electrons correspond to the red band shown in Fig. 1.3. An electron which does not interact with the foil is simply directed to the beam dump.

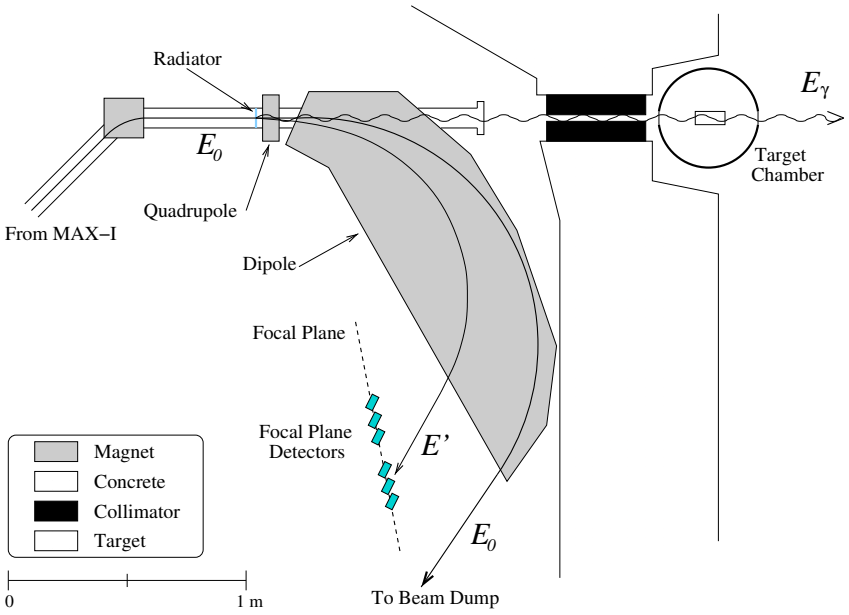

Figure 1.4: The photon-tagging process. Figure from Ref. [4].

1.4.3 Collimator

As a result of the extended electron beam, the bremsstrahlung process, and multiple scattering within the radiator, the photons emitted from the radiator will be distributed over an opening angle θ, as seen in Fig. 1.5. The photonuclear target is often placed several meters downstream of the radiator. In order to ensure that all photons have the possibility of hitting this target, a collimator is placed between the radiator and the target.

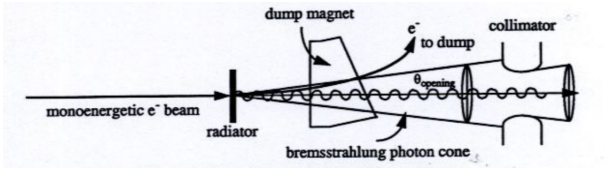

Figure 1.5: Collimation of bremsstrahlung photon beam. Figure from Ref. [3].

1.5 Focal plane

As previously discussed, a post-bremsstrahlung electron within the acceptance of the tagger magnet will bend from its original path, ideally onto the focal-plane. The focal-plane is shown in Fig. 1.6. It consists of 63 plastic scintillators, each connected to a PMT.

Figure 1.6: Focal-plane hodoscope used at MAX-lab. There are two sets of PMTs, each set belonging to one of the two scintillator planes.

The scintillator planes are set up in two rows, one containing 32 scintillators and the other 31 scintillators, so that an electron incident upon the focal-plane will ideally produce a signal in two of the focal-plane detectors simultaneously as it passes through both the front row and back row. Requiring this coincidence signal reduces background. Depending on the relative arrangement of the two scintillator planes with respect to one another, they may overlap by 50% or 100%, as shown in Fig. 1.7.

When an electron hits the focal-plane, the event is attributed to one of 64 'channels' based upon the coincidence between the front-plane and back-plane scintillators. In Fig. 1.7, the green areas represent coincidences corresponding to even channels, while the red areas represent coincidences corresponding to odd channels. An electron with an energy corresponding to the maximum energy subtended by the focal-plane will be registered in channel 0.

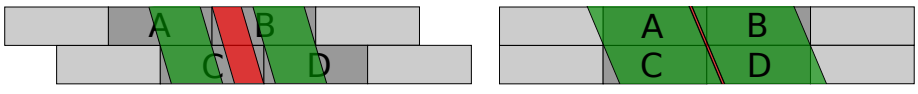

(a) 50% overlap mode (b) 100% overlap mode

Figure 1.7: Two possible overlap modes for the focal-plane. Mode (a) was used during the April 2012 experiments, while mode (b) was used during the June and September 2011 runs.

As shown in Fig. 1.7, the number of events corresponding to the odd channels will be very small compared to the number of events corresponding to the even channels in data from a run performed with 100% overlap mode. This is due to the much smaller recoil-electron phase space subtended by the odd channels using this configuration. When running in 50% overlap mode, the odd channels will contain many more events. However, the electrons do not hit the focal-plane perpendicularly, but rather at an angle less than 90°. Thus, the acceptance of the even channels will still be larger than that of the odd channels. The effect of the arrangement of scintillators can be seen clearly in the histograms corresponding to the number of hits in the focal-plane shown in Fig. 1.8.

1.6 Photon detectors

Two types of photon detectors were used for this project. For the time calibration of the focal-plane as well as for tagging-efficiency[1] measurements, a Pb-glass detector was used for low-rate in-beam measurements. For all other low-rate calibrations and high-rate scattering measurements, three NaI(Tl) detectors were used. The two main components of all three photon detectors used are large NaI(Tl) scintillation crystals and photomultiplier tubes. Although these two components are the same for the three detectors, they have been assembled with different configurations.

For complete details regarding the principles of operation for these detectors, see Appendix B.

1.6.1 Sodium Iodide detectors

Three NaI detectors were calibrated during this project:

- DIANA (Detector of Iodine and Sodium) from the University of Kentucky
- CATS (Compton And Two photon Spectrometer) from the University of Mainz
- BUNI (Boston University Sodium Iodide) from Boston University

DIANA detector

The DIANA detector consists of a single NaI(Tl) crystal with a diameter of 48 cm and a length of 51 cm. Around the core crystal, a 4 cm thick NaI(Tl) annulus has been placed. The annulus may be used as a cosmic-ray veto, but more importantly to 'catch' any of the EGS[2] that leaks from the core. The annulus is divided axially at its midpoint, and into sixths azimuthally, so that it consists of 12 segments in total. 19 PMTs are attached to the core, and 36 PMTs

[1] The tagging effciency is defined as the ratio of photons striking the photon detector to the number of electrons incident on the focal plane.

[2] *Electron Gamma Shower*. See Appendix B for a complete discussion.

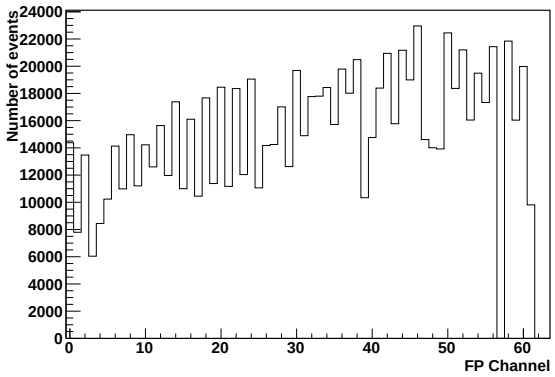

(a) 50% overlap mode run from April 2012.

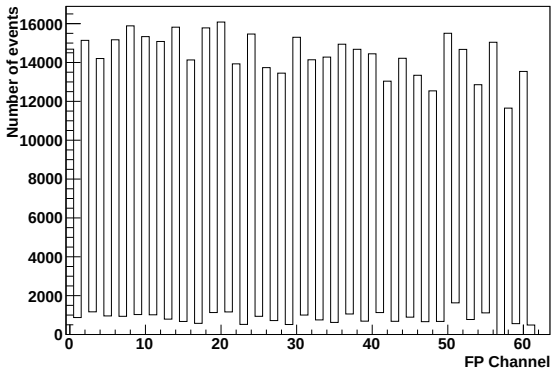

(b) 100% overlap mode run from September 2011.

Figure 1.8: Focal-plane histograms for different focal-plane overlap modes. Note that for 100% overlap mode, there is a clear 'picket fence' appearance of the histogram, as the odd channels contain many fewer events than the even channels. When running in 50% overlap mode, the number of events in the odd channels is much higher, although still less than in the even channels. This is explained by the 'odd-even effect' described in the text. Note also that during the runs, focal-plane channel 57 was broken, and therefore the corresponding bin in the histograms has zero entries (both for 50% overlap and 100% ovelap).

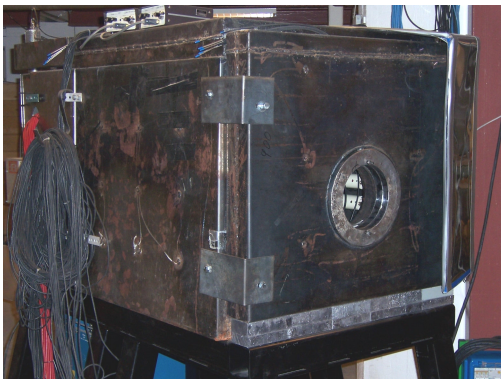

Figure 1.9: Photo of DIANA, showing the shielded detector without cosmic-ray veto scintillators. Figure from Ref. [5].

are attached to the annulus. The 19 core PMTs and half of the annulus PMTs are attached to the rear of the detector, while the other half of the annulus PMTs are attached to the front of the detector.

The entire detector is shielded by 10 cm of lead to prevent background radiation from reaching the scintillators. It is also covered by six 6 mm thick plastic-scintillator paddles acting as cosmic-ray vetoes. A cosmic ray going through the detector will give a coincidence signal in veto scintillators placed opposite of each other (since a cosmic ray will pass through the detector in a straight path).

CATS detector

The CATS detector contains a NaI(Tl) core crystal which, with a diameter of 26.7 cm and a length of 63.5 cm, is considerably smaller than the DIANA core. In addition, CATS contains six annular NaI(Tl) segments of thickness 10.8 cm, placed around the core as seen in Fig. 1.12. Surrounding these segments, as well as on the back of the detector, a 10 cm thick plastic scintillator acts as a cosmic-ray and charged-particle veto. A cosmic ray going through the detector will give a coincidence signal in veto scintillators placed opposite of each other (since a cosmic ray will pass through the detector in a straight path). The cylindrical plastic veto is divided into five segments, as seen in Fig. 1.12. A total of 50 PMTs are attached to the detector: 7 to the core, 4 to each NaI(Tl) segment, 3 to each plastic segment, and 4 to the plastic veto at the back of the detector.

The entire detector is shielded by a 10 cm thick layer of lead to prevent background radiation from reaching the scintillators. Also, a 1 cm layer of $^{6}Li_2CO_3$ is placed between the NaI(Tl) segments and the plastic-scintillator segments to absorb low-energy neutrons. Finally, a plastic-scintillator veto covers the detector aperture.

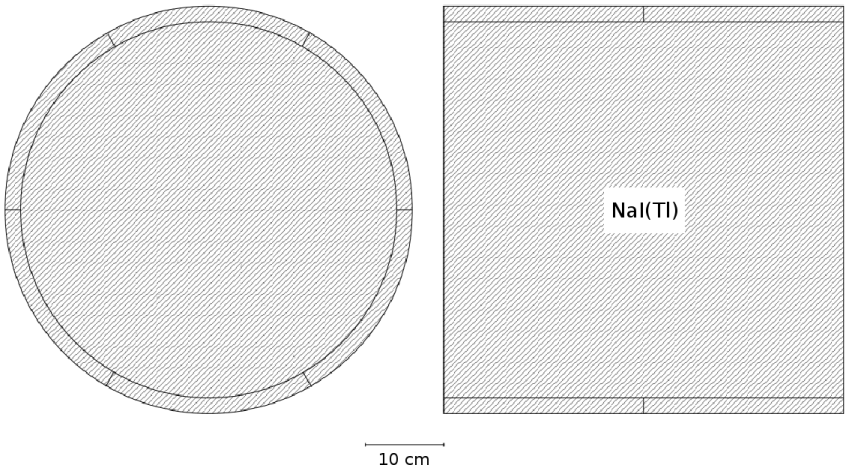

Figure 1.10: Schematic drawing of the DIANA detector. The left figure shows a cross section of the detector from the front/back, and the right figure shows a cross section of the detector from the side. Figure from Ref. [6].

Figure 1.11: Photo of the CATS detector. Figure from Ref. [7].

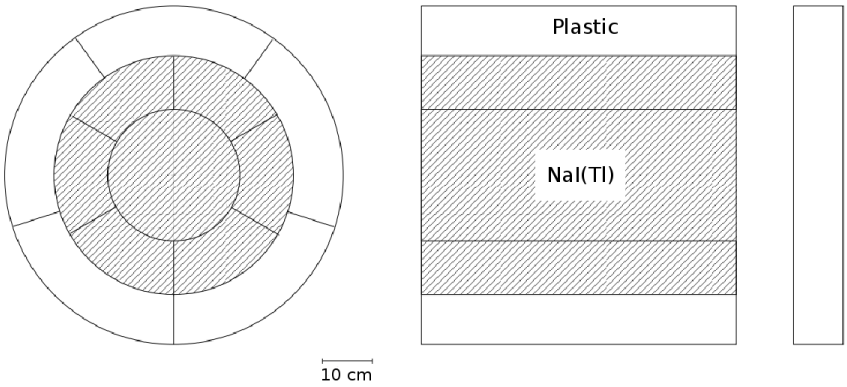

Figure 1.12: Schematic drawing of the CATS detector. The left figure shows a cross section of the detector from the front/back, and the right figure shows a cross section of the detector from the side. Figure from Ref. [6].

BUNI detector

BUNI is rather similar to CATS in its design, as seen in Fig. 1.14. It consists of a core NaI(Tl) crystal of diameter 26.7 cm and length 55.9 cm. Around this, four 11.4 cm thick segments of NaI(Tl) are placed, which are usually referred to as quadrants, or 'quads'. Surrounding the quads is a 12.7 cm thick BC-400 plastic scintillator, divided into six segments. This scintillator is employed as a cosmic-ray veto. A cosmic ray going through the detector will give a coincidence signal in veto scintillators placed opposite of each other (since a cosmic ray will pass through the detector in a straight path). In total, 31 PMTs are attached to BUNI: 7 to the core, 3 to each NaI(Tl) quad, and 2 to each plastic segment.

The entire detector is shielded by a 10 cm thick layer of lead to prevent background radiation from reaching the scintillators. Also, a 5 mm thick plastic scintillator covering the detector aperture is used as a charged-particle veto.

1.6.2 Pb-glass detector

As previously mentioned, a Pb-glass detector is used for two parts of the experiment: tagging-efficiency measurements and focal-plane calibrations.

When a photon enters this detector, an electromagnetic shower is started. Pb-glass is a material with a very high refractive index, making it possible for the particles in the shower to exceed the speed of light. As explained in App. B.1.2, a particle moving faster than light in a medium causes a light flash (Čerenkov radiation) that is proportional to the energy of the original photon entering the detector. A single PMT is connected to the Pb-glass detector. Due to the low rates used during Pb-glass runs, it is not shielded from background radiation.

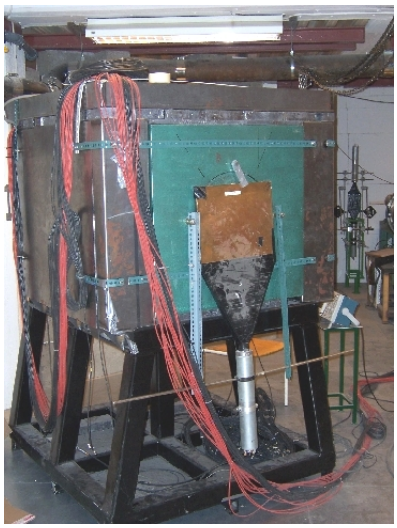

Figure 1.13: Photo of the BUNI detector. Figure from Ref. [8].

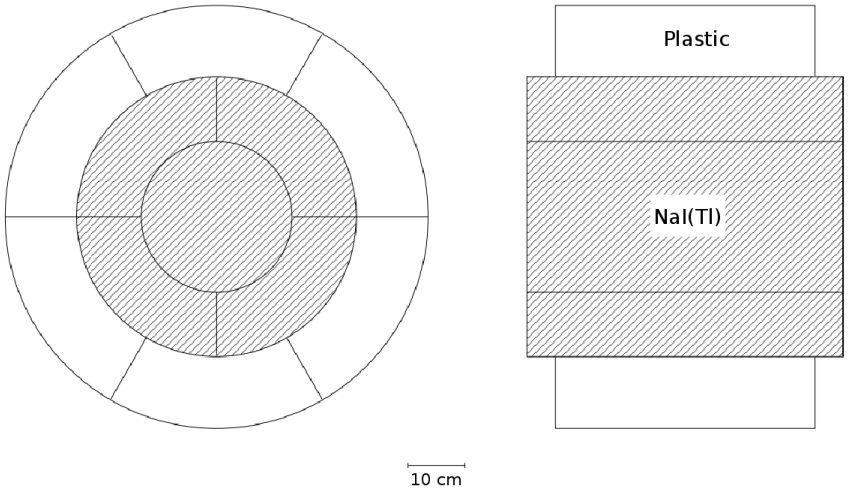

Figure 1.14: Schematic drawing of the BUNI detector. The left figure shows a cross section of the detector from the front/back, and the right figure shows a cross section of the detector from the side. Figure from Ref. [6].

Figure 1.15: Photo of the Pb-glass detector. Figure from Ref. [9].

1.7 Trigger modes

As previously mentioned, there are two main experimental components: the focal-plane hodoscope and the photon detector. The photon detector can be DIANA, BUNI, CATS or the Pb-glass detector. For a tagged-photon event to have occured, an electron must be detected at the focal-plane hodoscope in coincidence with a photon in the photon detector. Trigger electronics are used to determine whether or not this has happened. The trigger electronics are generally configured in two different modes: 'FP OR' trigger or 'photon-detector' trigger.

For complete details describing how the crucial components of the trigger electronics actually function, see Appendix C.

1.7.1 FP OR trigger

When the electronics are run in FP OR trigger mode, an electron hitting any one of the focal-plane channels provides the event trigger that starts the TDCs and gates the QDCs, as seen in the schematic overview of the electronics in Fig. 1.17.

When an electron hits any of the focal-plane scintillators, an analog electronic signal is produced at the anode of the corresponding PMT. This is sent to a discriminator, which, provided that the analog pulse is above the discriminator threshold, creates a digital signal. This signal is replicated with a logic fanout module and then sent to a scaler, a logical OR module, and (with sufficient delay) as a stop signal to a TDC. The logical OR module is fed by signals from all focal-plane channels, and thus gives an output signal whenever any one of the focal-plane channels is hit. This signal is sent to a master-trigger unit, and then to a LATCH, which simultaneously enables data collection and disallows further input signals until the event has been fully processed. A logic fanout module then replicates the LATCH signal, so that the QDC gate is opened, the

focal-plane TDCs are started, and the DAQ computer is enabled.

Figure 1.16: Overview of the electronics when using the FP OR trigger. Figure from Ref. [3].

As seen in Fig. 1.17, in FP OR trigger mode, the TDC is started by the exact same signal that stops it (with appropriate delays). This means that the time between the TDC start and stop signals is completely determined by the cable delays for the specific focal-plane channel - a so-called 'self-timing' peak.

While the QDC gate is open, any event in the photon detector will result in a signal for the QDC to integrate. Therefore, if the photon corresponding to the bremsstrahlung electron triggering the electronics is collimated away (and thus does not reach the photon detector), the QDC will have no signal to integrate. Should this happen, the event will fall into the QDC bin corresponding to a 0 MeV energy deposition. This is known as a 'pedestal' event.

1.7.2 Photon-detector trigger

When a photon detector is used as the trigger, a detected photon provides the event trigger that starts the TDCs and gates the QDCs.

A photon entering a photon detector will give rise to an analog pulse from the central PMT in the detector. This analog pulse is replicated using a linear fanout module. One of the resulting signals is delayed, and is passed directly to a QDC, while the other goes to a discriminator. Provided that the pulse height is above the discriminator threshold, a digital signal is produced. This signal is sent to a master trigger unit, and further on to a LATCH. The signal from the LATCH is sent to a logic fanout module, which produces three copies: one to gate the QDCs, one to start the TDCs, and one to enable the DAQ.

At the same time, an electron related to this photon might be detected at the focal-plane. This results in an analog signal which is sent to a discriminator. The discriminator sends out two digital signals: one to a scaler, and one to stop

Figure 1.17: Overview of the electronics when using the photon-detector trigger. Figure from Ref. [3].

the TDC for the focal-plane channel that was struck.

1.7.3 Trigger differences

Four main differences between the trigger modes are evident:

- TDCs
  - when running in FP OR trigger mode, the time between the start and stop signals to the focal-plane TDCs is solely determined by cable lengths within the the electronics since the same signal both starts and stops the focal-plane TDCs. Thus, relative-timing differences between the focal-plane channels due to small variations in cable lengths may not be identified.
  - when running in photon-detector trigger mode, a single photon detector provides the start to the focal-plane TDCs while the stops come from electrons detected individually by the focal-plane detectors. Thus, relative-timing differences between the focal-plane channels due to small variations in cable lengths may be identified.
- QDCs
  - when running in FP OR trigger mode, the QDC may not get any signal to integrate since the photon may not reach the detector, while the QDC is gated by a hit in the focal-plane. Thus, pedestals may be identified. Pedestals consist of events where no photon was detected, but the electronics were triggered by an electron at the focal plane.
  - when running in photon-detector trigger mode, there will always be a signal to integrate, since the QDC is gated by the detection of a photon. Thus, pedestals may not be identified.

Chapter 2

Analysis

In order to use the focal-plane and the NaI(Tl) photon detectors in an experiment, calibrations must be performed. To do this, each of the photon detectors are placed individually in the path of the photon beam and data are collected. These runs are commonly called *inbeam calibration runs*.

In this chapter, a summary of an inbeam calibration will be presented. For complete details regarding the data-analysis software, see Appendix D.

2.1 TDC offset calibration

As previously discussed, the time between the start and stop of the focal-plane TDCs depends on the delay-cable lengths. As these are slightly different for each of the 64 focal-plane channels, a photon event with an electron in one focal-plane channel will not generate a TDC peak at the same position as an event at another channel. Each bin of the TDC has a width of around 300 ps, whereas the propagation of a signal through a 1 meter delay cable is about 5 ns. Thus, even small differences in cable length can clearly be seen.

Since the time between the detection of a photon and the detection of an electron is of interest, the photon-detector trigger must be employed. As for the choice of photon detector, any of the NaI detectors or the Pb-glass detector may be used. The advantage of using the Pb-glass detector is that it has a smaller volume than any of the three NaI detectors. Also, many tagging-efficiency runs (where the Pb-glass detector is used) are performed during a given experiment. This makes it possible to see variations in the TDC offsets, which are indicative of major problems with the experiment apparatus.

Due to the design of the tagger and focal-plane electronics, a photon/electron coincidence should be separated by a time that is constant and independent of focal-plane channel. However, due to the small timing differences already mentioned, as well as differences between the conversion gains of the different single-hit TDCs, there is a slight difference in the positions of the coincidence peaks corresponding to the different channels. The multiple TDC peaks making

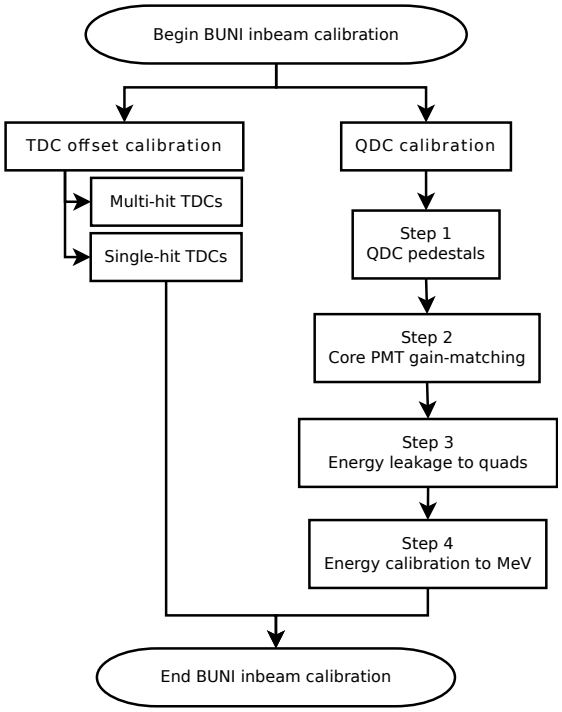

Figure 2.1: Overview of the BUNI inbeam data analysis.

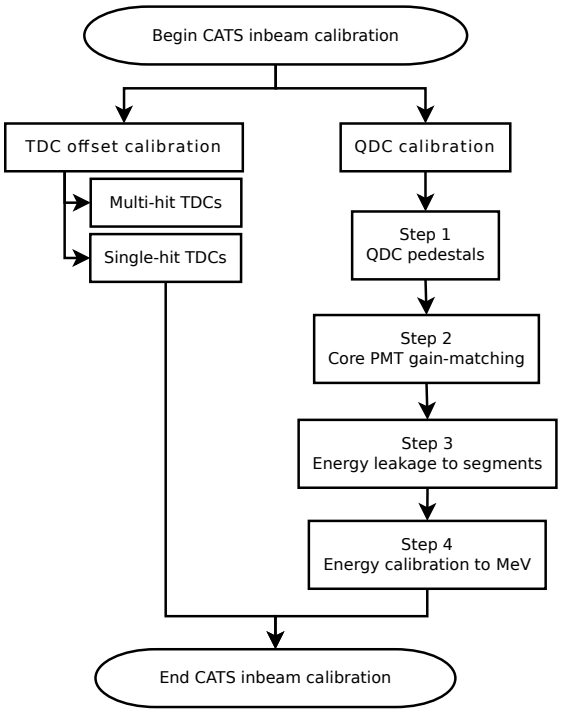

Figure 2.2: Overview of the CATS inbeam data analysis.

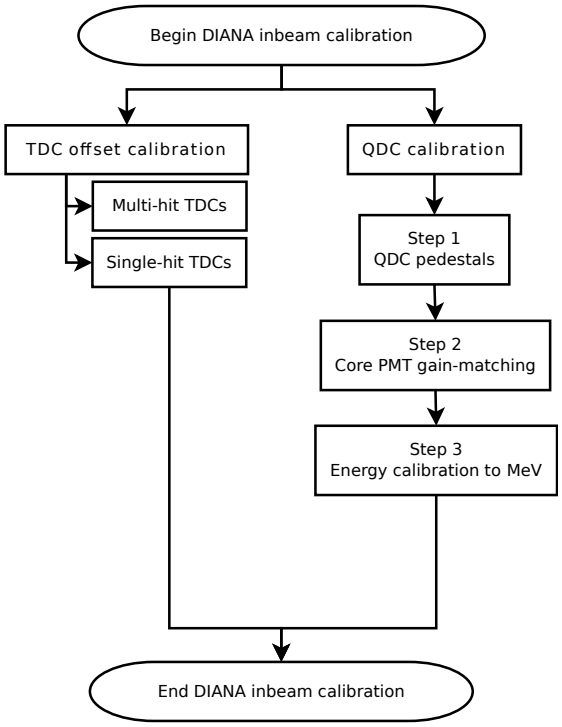

Figure 2.3: Overview of the DIANA inbeam data analysis.

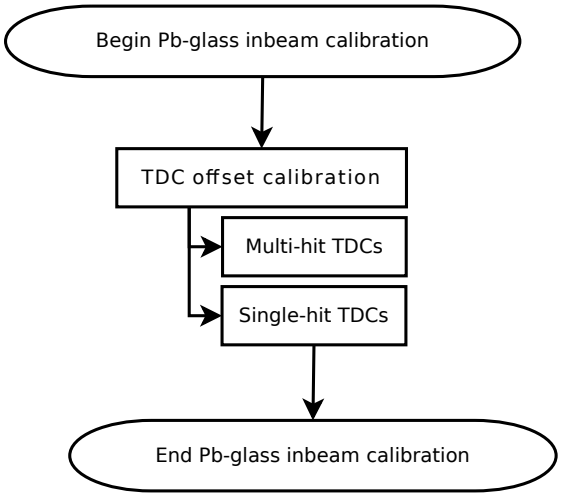

Figure 2.4: Overview of the Pb-glass inbeam data analysis.

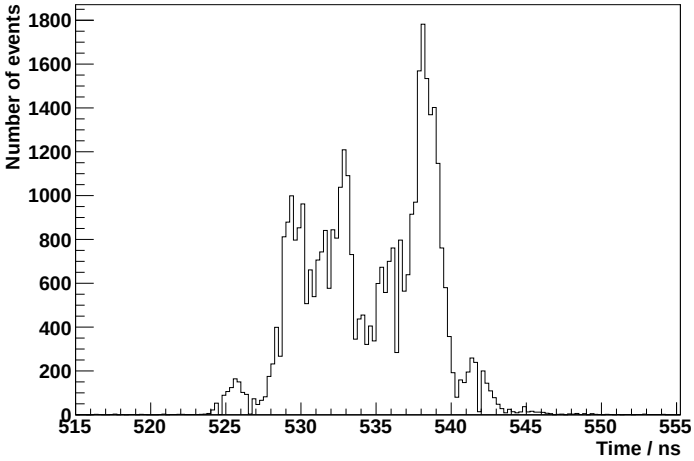

(a) Summed raw single-hit TDC spectra

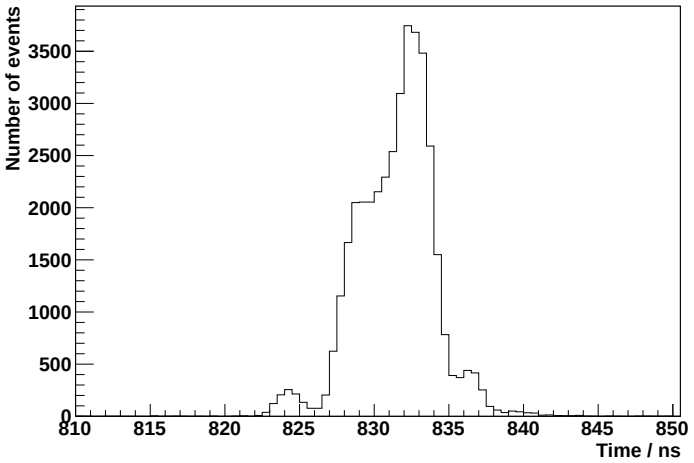

(b) Summed raw multi-hit TDC spectra

Figure 2.5: Comparison between raw single- and multi-hit TDC spectra, summed over all 64 focal-plane channels.

up the spectra seen in Fig. 2.5 have to be located and repositioned.

In order to collect the many different TDC peaks into one sharp 'summed' peak, the positions of the individual peaks must first be determined. This is done by looking at the raw TDC peak for each focal-plane channel, and fitting a Gaussian distribution to the peak, as in Fig. 2.6. The mean μ of the Gaussian is taken to be the location of the TDC peak.

2.1.1 Single-hit TDCs

As previously mentioned, there is a difference in the gain for each of the single-hit TDC channels. Thus, a correction must be applied to all the data, so that the positions of the timing peaks for all of the focal-plane TDCs differ only because of the different delay-cable lengths. More specifically, each single-hit focal-plane TDC has a corresponding calibration constant (in ps/channel), with which the peak position (measured in channels) must be corrected. This enables one to compare all TDC channels easily as they all have ns as units.

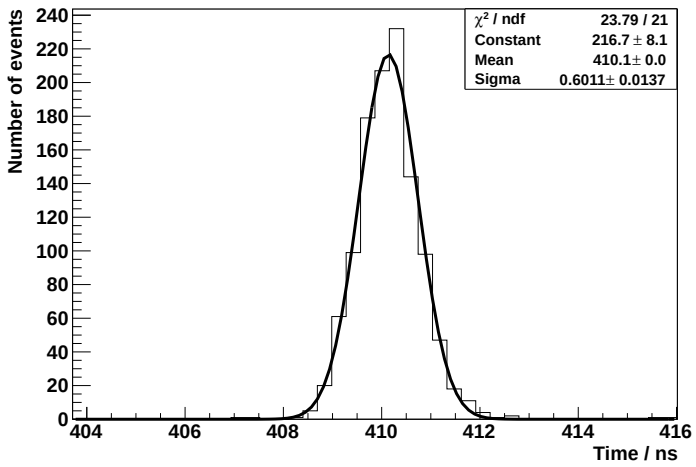

Figure 2.6: TDC peak containing all photon coincidences with an electron detection in focal-plane channel 16. A Gaussian distribution has been fitted to the data. The mean of the Gaussian is taken to be the peak location.

After the gain correction of the single-hit TDCs, a Gaussian is fitted to each of the 64 focal-plane TDC peaks. In doing this, a set of offset values corresponding to the mean of the Gaussian distributions is obtained. By subtracting this corresponding offset value from each focal-plane channel peak, and then adding a constant offset for all channels, all peaks may be relocated to a user-definded position. The result of the gain-corrections and the peak relocation based on the individual peak positions can be seen in Fig. 2.7.

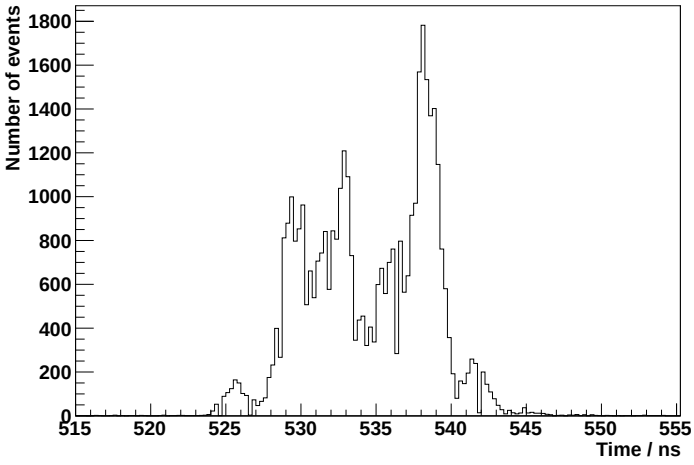

(a)

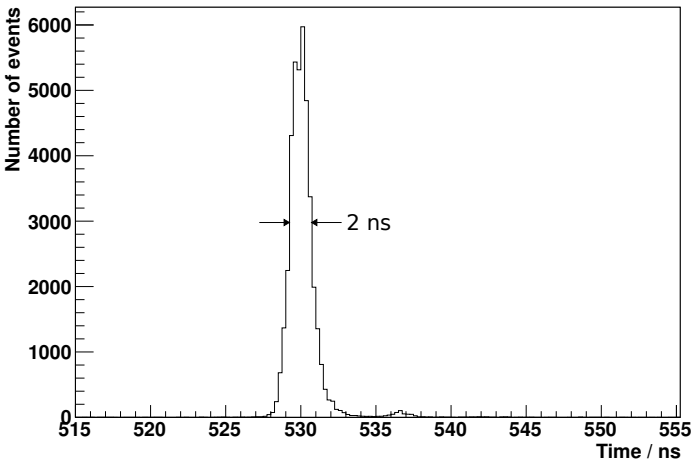

(b)

Figure 2.7: Summed single-hit TDC spectrum (a) before offset- and gain-correction and (b) after offset- and gain-correction. The effect of the corrections is striking.

By comparing the histograms, the effect of the single-hit TDC calibration can be seen clearly. More exactly, the uncalibrated TDC sum spectrum has multiple peaks spread out over about 20 ns, while the corrected spectrum has a FWHM value of about 2 ns.

2.1.2 Multi-hit TDCs

In contrast to the single-hit focal-plane TDCs, no gain correction is performed for the multi-hit TDCs. This is because each channel of the multi-hit TDC has essentially the same gain. Thus, only the peak-position differences due to differences in delay-cable lengths have to be corrected. This is done in the same way as for the single-hit TDCs - by fitting a Gaussian to each focal-plane peak. The resulting summed peaks can be seen in Fig. 2.8.

By comparing the histograms, the effect of the multi-hit TDC calibration can be seen clearly. More exactly, the uncalibrated TDC sum spectrum has multiple peaks spread out over about 20 ns, while the corrected spectrum has a FWHM value of about 2 ns.

2.2 QDC calibration

Depending upon the trigger used, the QDC spectra corresponding to the photon detector PMTs will look different. If the FP OR trigger is used, there is a possibility that an event is triggered without the bremsstrahlung photon actually reaching the detector, as explained previously[1]. Should this happen, there will be no current at the PMT anode associated with the photon for the QDC to integrate, and therefore there will be an event corresponding to zero deposited charge, the pedestal.

This zero-charge peak can be seen as the leftmost peak in Fig. 2.9, which shows the QDC spectrum for the central BUNI PMT using the FP OR trigger. Two other important features of the QDC spectrum are also presented - the 'gain' peak and the 'overflow' peak. The gain peak is the rather broad peak in the center of the spectrum corresponding to tagged photons, and the overflow peak is the rightmost peak. The overflow peak contains all events where the deposited energy was higher than the maximum limit of the QDC.

2.2.1 QDC pedestals

As previously mentioned, a detected electron may correspond to a photon that does not reach the photon detector. Should this happen, the QDC will be gated, but no energy will be deposited in the photon detector resulting in no current for the QDC to integrate. When all events are summed together, these zero-charge events will form a peak - the QDC pedestal. These events can be recorded, as previously stated, when using the FP OR trigger. The pedestal peak can be made even more visible by triggering on a detector other than the

[1] Due to collimation, for example.

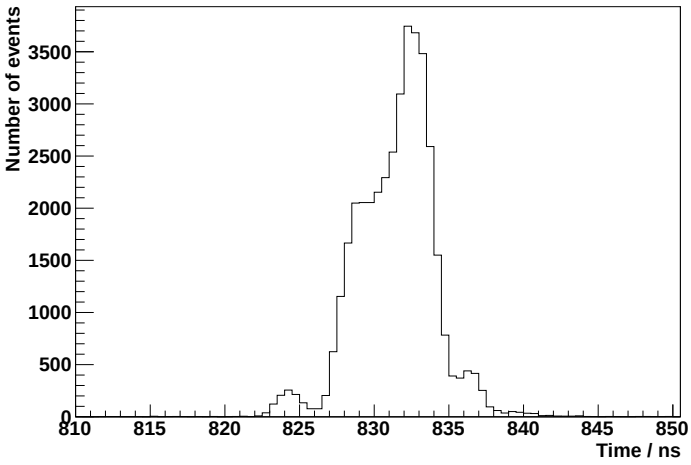

(a)

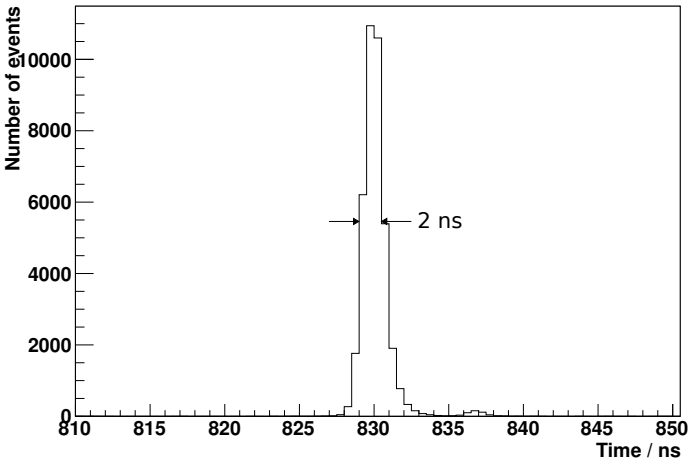

(b)

Figure 2.8: Summed multi-hit TDC spectrum (a) before offset correction and (b) after offset correction. The effect of the correction is striking.

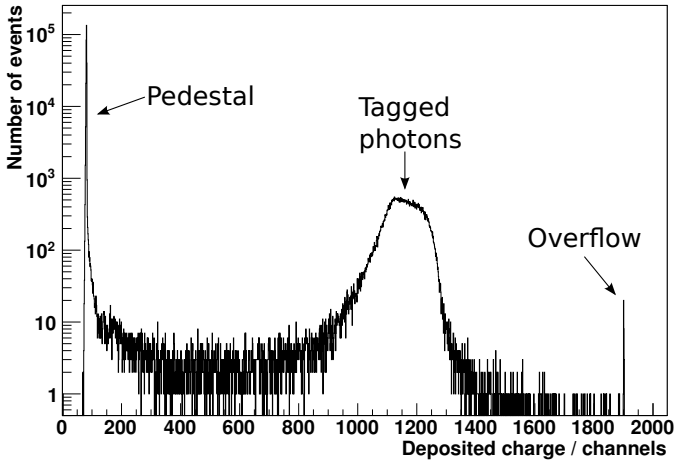

Figure 2.9: QDC spectrum for the central BUNI PMT obtained using the FP OR trigger. This spectrum contains events from all 64 focal-plane channels.

one being analysed. For example, the BUNI pedestal spectra can be studied when CATS is in the beam. In this case, no photons at all will reach BUNI, but the electronics will be triggered when a photon enters CATS. Therefore, almost all of the events in the BUNI QDC spectrum will be at a position corresponding to zero-energy deposition, and the pedestals will be very clear.

For an event where there is no photon but the electronics are triggered, the energy deposited in each PMT in the photon detector is zero. Because of the slightly different settings on the electronics connected to each of the PMTs, the QDC channel value corresponding to a zero-energy deposition in one PMT will be slightly different from the zero-energy channel for another PMT. This can be clearly seen when extracting the pedestal peaks from QDC spectra of different PMTs, as shown for BUNI PMTs 1 to 5 in Fig. 2.10a.

In order to locate the pedestal for each of the PMTs, a Gaussian distribution is fitted to each pedestal. An example of a Gaussian fit to data is seen in Fig. 2.6. The mean μ of the Gaussian is a measure of the position of the pedestal peak. By repeating this for every PMT in the detector, the different pedestals may be determined. The result is an array containing one offset value for each detector PMT (11 in the case of BUNI). By subtracting these values from the pedestal-peak positions and then adding a constant offset, the pedestals may all be calibrated to the same position, as shown in Fig. 2.10b. Note that although the pedestal corresponds to no deposited energy in the photon detector, the peak has been placed arbitrarily in channel 100 for increased clarity.

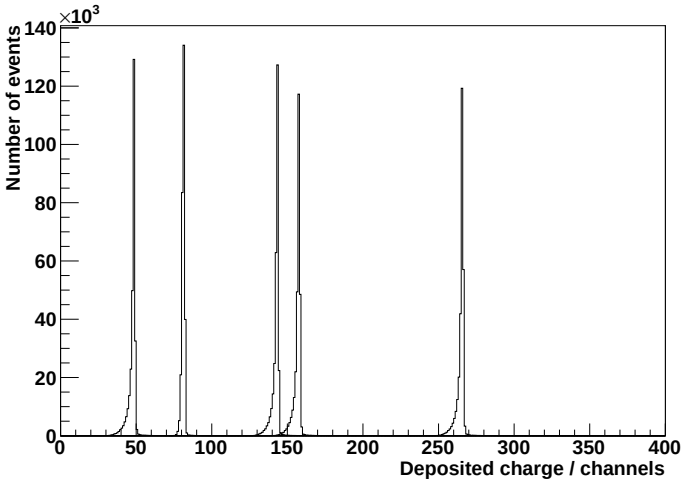

(a)

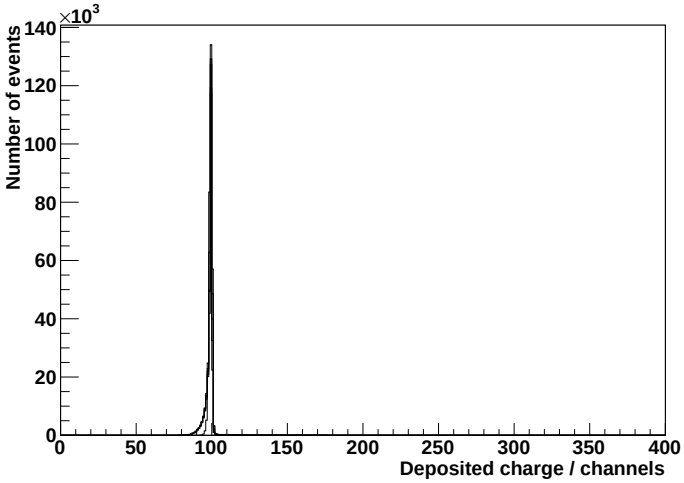

(b)

Figure 2.10: Five of the BUNI PMT pedestals (a) before and (b) after calibration.

2.2.2 Core gain matching

Although the pedestals from the QDC were determined in the previous section, the gains from the different PMTs also have to be matched.

The gain of the QDC spectrum may be determined from the location of the tagged-photon peak. Figure 2.11 shows pedestal-corrected gain peaks corresponding to events with electrons hitting focal-plane channel 1 for two different PMTs. Clearly, the peak positions are different even when the pedestal value has been subtracted.

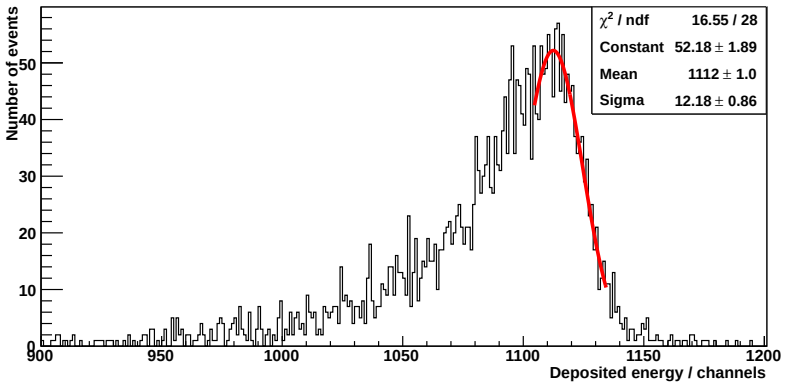

(a)

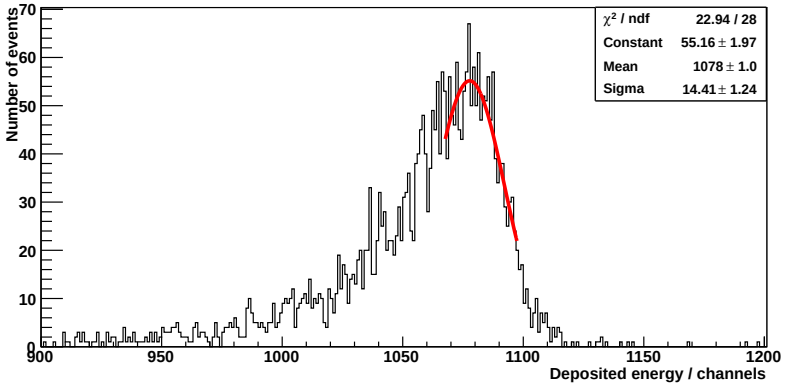

(b)

Figure 2.11: Gain peaks for two of the BUNI core PMTs, with pedestal values subtracted. A Gaussian distribution has been fitted to the peak regions to determine their locations.

As seen in Fig. 2.11, a Gaussian distribution is fitted to the peak. The mean of this Gaussian is a measure of where a certain deposited photon energy (as

determined from the focal-plane channel) is located, and this can be evaluated for each of the core PMTs.

For each core PMT for every tenth focal-plane channel (focal-plane channels 1, 11, 21, 31, 41, 51, 61), the location of the tagged-photon peak in the corresponding QDC was determined using a Gaussian fit. From the fit means, the peak positions for each tagger channel investigated were determined relative to those of the central core PMT by dividing their fit means by the fit mean of the central core PMT. This resulted in seven independent extractions of the gains of each of the core PMTs - one for each tagger channel investigated. By taking the average of these seven values, a global gain relative to the central core PMT was obtained for each core PMT.

By correcting the inbeam spectrum for each PMT with its corresponding relative-gain value, the inbeam spectrum for each PMT may be aligned to a single location, thus enabling a single gain-matched and offset-corrected central core spectrum to be formed. Now, an event where an electron hits a certain focal-plane channel will result in a gain peak at a position that is independent of PMT, as shown in Fig. 2.12.

The result of the gain matching can be seen even clearer on looking at the sum of the energy depositions in all core PMTs. The summed distribution for a photon corresponding to an electron event in focal-plane channel 1 before and after core gain matching is seen in Fig. 2.13.

Positions of core-summed spectra peaks

This analysis step resulted in 64 spectra (one for each focal-plane channel), each containing an energy distribution summed over all core PMTs. The peak of each spectrum (as the one shown in Fig. 2.13b) corresponds to a certain photon energy deposited in the core PMTs of the detector. The summed-peak position may be determined via a Gaussian fit. When doing this for all focal-plane channels, an array containing 64 values may be obtained.

2.2.3 Energy leakage to quads/segments

The DIANA detector consists of only one NaI crystal, which is the core, while BUNI and CATS do not. As discussed in Sec. 1.6, CATS has six outer segments and BUNI has four outer quads. When a highly energetic photon enters the detector, the resulting EGS (see Fig. 2.14) may leave the core crystal. If this happens, not all of the energy of the photon is deposited in the core. If the EGS leaks into a single quad/segment, the 'edge effect' illustrated in Fig. 2.15 results. Thus, the energy detected in the non-core part of the detector must be calibrated and then added back into the core spectrum. This is done by comparing the detected energy in a non-core crystal for an event with the energy detected in the core for the same event, as seen in Fig. 2.15.

Regardless of the detector chosen, the total EGS of the tagged photon will be contained by the total detector volume. Thus, the detected tagged-photon energy will be fixed.

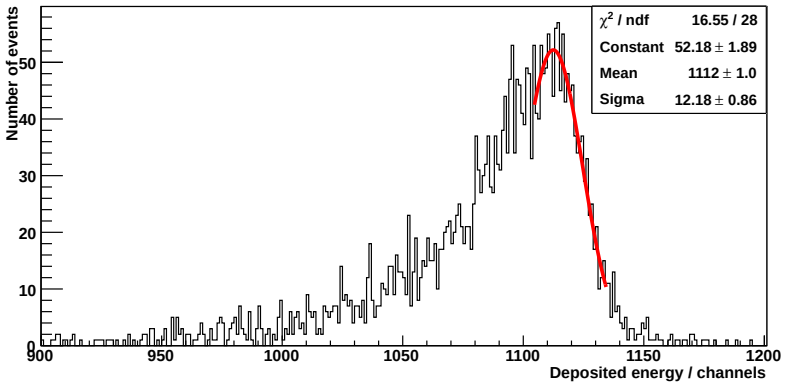

(a)

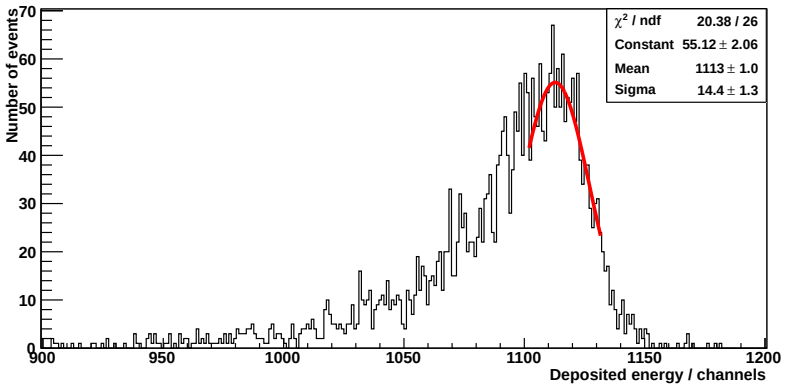

(b)

Figure 2.12: Gain peaks for the same BUNI core PMTs as shown in Fig. 2.11, with pedestal values subtracted and gain matching performed.

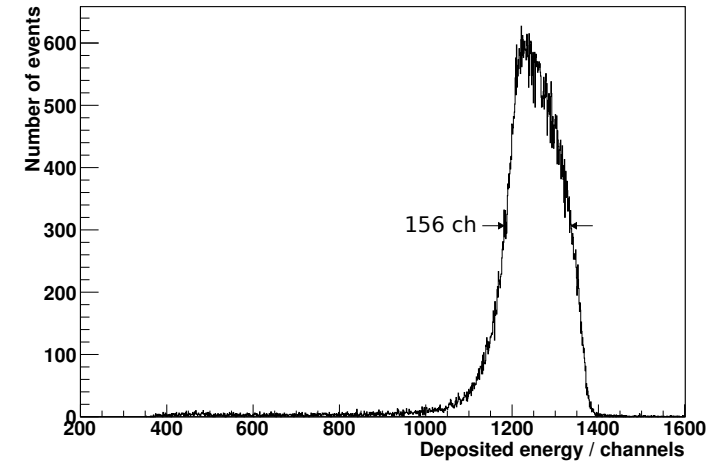

(a) Before gain matching

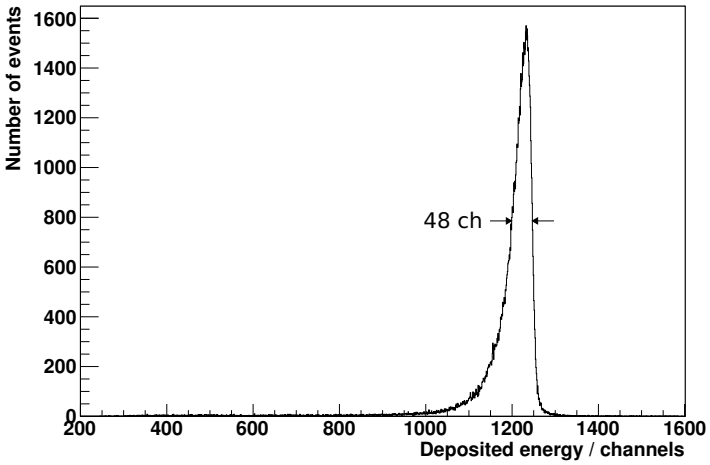

(b) After gain matching

Figure 2.13: Total energy-deposition peak for the BUNI core, before and after core gain matching. The arrows illustrate the peak FWHMs.

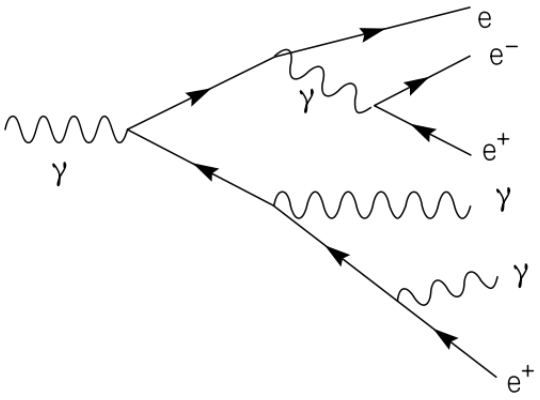

Figure 2.14: Feynman diagram of the beginning of an EGS. A highly energetic photon produces a shower of photons and electrons/positrons. Figure from Ref. [10].

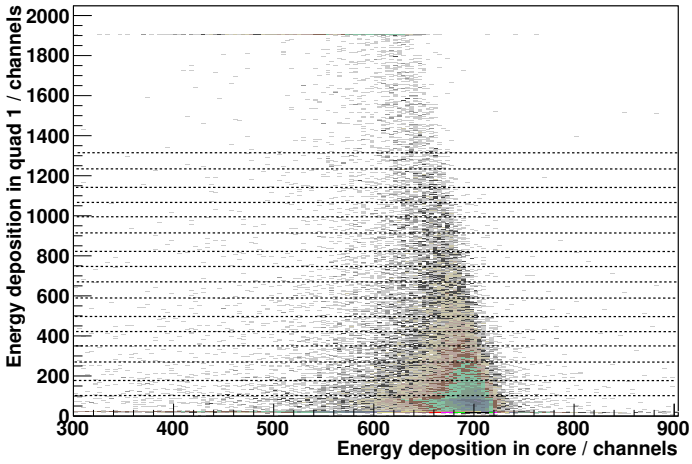

Figure 2.15: Energy deposition in BUNI quad 1 versus the energy deposition in the core crystal. The dashed lines indicate the orientation of the 'slices'. See text for details.

When calculating the energy deposition in the core for Fig. 2.15, the corresponding core inbeam peak position from the previous section has been subtracted from each event. After doing this, the event is positioned at channel 700 on the horizontal axis. Doing this for all events gives a two dimensional histogram, where the z axis corresponds to the number of events. Because of the subtraction of the inbeam peak position and subsequent repositioning of the events, a point in Fig. 2.15 with a position on the horizontal axis below 700 represents an event where the energy deposition in the core is below what is expected if the tagged photon only gives an energy deposition in the core[2].

To obtain a useful relation between the energy depositions, the histogram in Fig. 2.15 is 'sliced' along the horizontal axis. The slices are then projected onto one-dimensional histograms, to which Landau distributions (seen in Fig. 2.16) are fitted. The peak positions for all slices are then located, and a straight line is fitted to them as seen in Fig. 2.17.

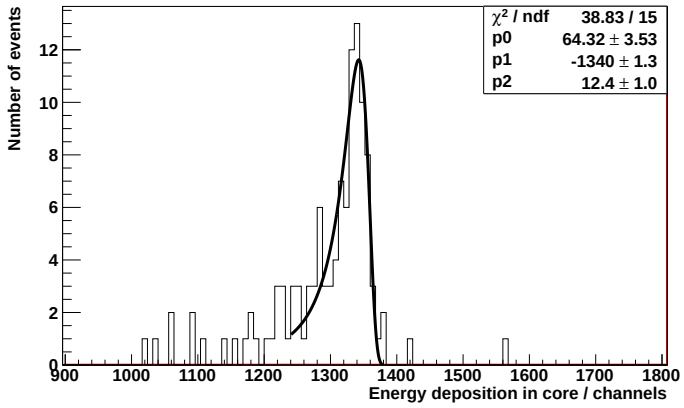

Figure 2.16: Example of a Landau fit to a slice of the scatter plot in Fig. 2.15.

When fitting a Landau to each slice, a set of peak values is obtained (one fit peak position for each slice). To these values, a straight line is fitted, as seen in Fig. 2.17. This linear fit is used to relate the energy deposition in the core to the energy deposition in each quad/segment.

When the plot and fit are reversed so that the energy in the core is the dependent variable, the slope of the line is a measure of how much the energy deposition in the core decreases as the energy deposition in the respective quad increases. The negative of this slope is used to obtain the energy deposition in each of the quads/segments:

$$E_{tagged} = E_{core} + kE_{quad/segment} \tag{2.1}$$

[2]That is, some of the EGS has leaked out of the core.

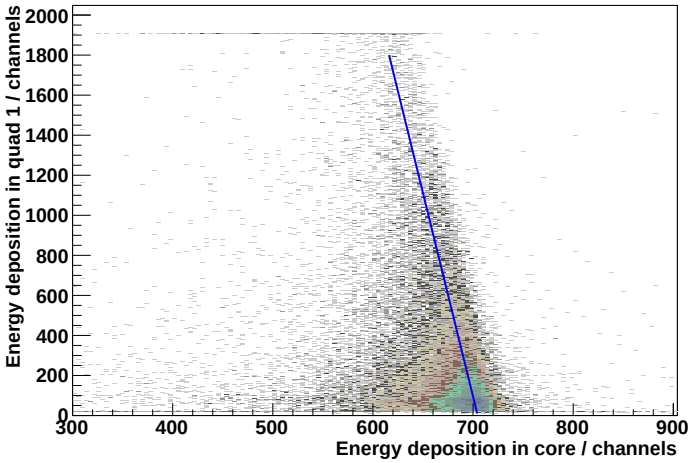

Figure 2.17: Energy deposition in BUNI quad 1 versus the energy deposition in the core crystal. A straight line has been fitted to the data. See text for details.

$$E_{quad/segment} = (E_{tagged} - E_{core})\frac{1}{k} \tag{2.2}$$

$$E_{quad/segment} = -\frac{E_{core}}{k} + \frac{E_{tagged}}{k} \tag{2.3}$$

where
E_{tagged} = Tagged-photon energy, known from focal-plane channel
E_{core} = Energy deposition in core
k = Negative of the inverse slope of the linear fit in Fig. 2.17
$E_{quad/segment}$ = Energy deposition in quad/segment

This way, the energy deposition in each quad/segment is calculated and may be added back into the energy deposition in the core. By adding this to the energy deposited in the core from Sec. 2.2.2, the position of the total gain peak is obtained.

Positions of core/segment-summed spectra peaks

This analysis step resulted in 64 spectra, each containing an energy distribution summed over all core and quad/segment PMTs. The peak of each spectrum (as the one shown in Fig. 2.13b) corresponds to a certain photon energy deposited in *all* of the PMTs of the detector. The summed-peak position may be determined via a Gaussian fit. When doing this for all focal-plane channels, an array containing 64 values may be obtained.

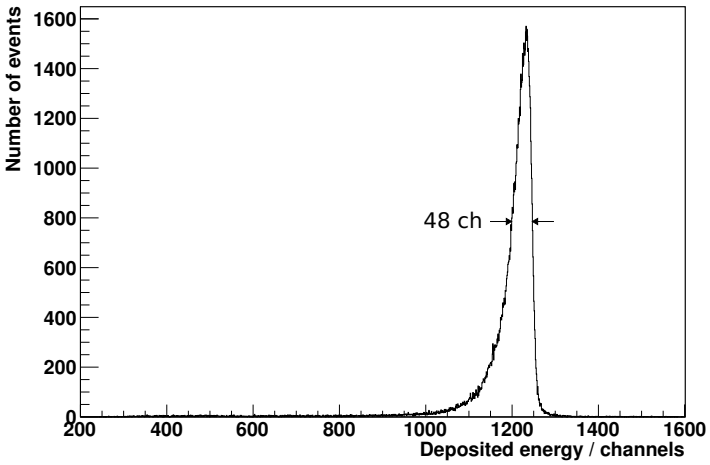

(a) Core summed energy peak

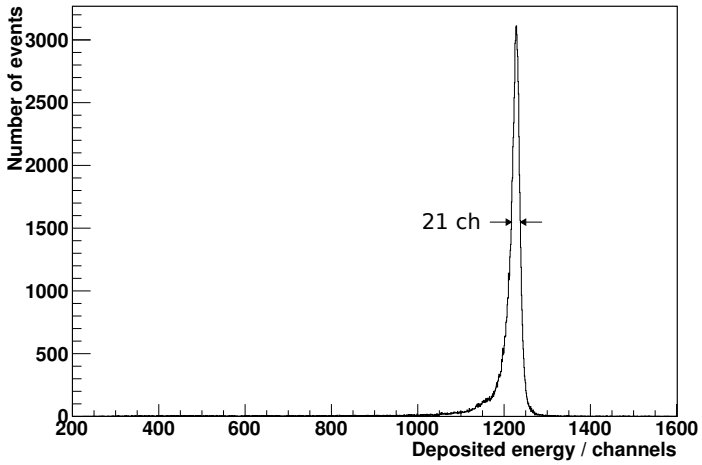

(b) Core and quad/segment summed energy peak

Figure 2.18: Comparison between the energy peak corresponding to the total deposited energy in the (a) core after core gain matching and (b) core and quads/segments after core gain matching and quad/segment deposition addback. The arrows illustrate the peak FWHMs.

2.2.4 Energy calibration of spectra

Although the relative energy of a bremsstrahlung photon corresponding to an electron hitting a specific focal-plane channel (a 'tagged' photon) was determined by matching the gains of all PMTs, the absolute energy scale has not yet been converted from QDC channels to MeV. Thus, a calibration relating QDC channels to energy is needed for the results in Sec. 2.2.3.

From the Lorentz force (Eq. 1.2), the path of an electron of any energy due to the magnetic field from the tagger magnet can be determined. This can be related to the energy of the photon from the bremsstrahlung process corresponding to any given focal-plane channel. Thus, if the electron-beam energy is known there results a set of known photon energies corresponding to each of the focal-plane channels. There is also a set of calibrated photon energies (measured in QDC channels) resulting from the inbeam measurements (recall the previous sections of this thesis). When plotted against each other, the linear relationship between the two is clear, and a straight line can be fitted as shown in Fig. 2.19.

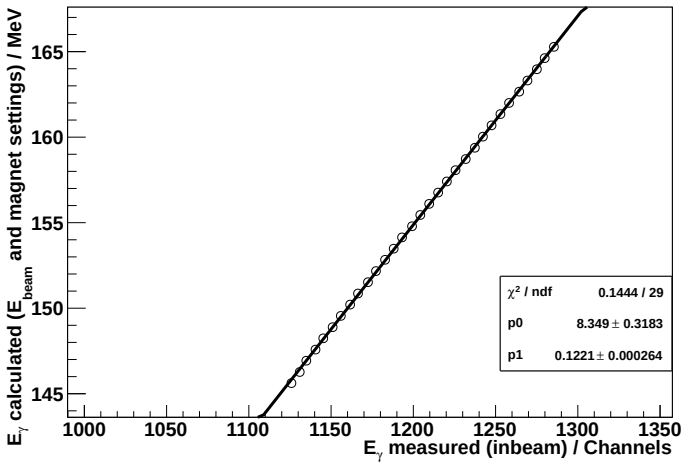

Figure 2.19: Plot of the calculated photon energy (dependent on the electron-beam energy, the tagger magnet, and the focal-plane setup) in MeV as a function of detected energy in QDC channels. A straight line has been fitted, and the resulting parameters are used as a gain-calibration curve.

The fit equation is the relation between the deposited energy and the photon energy predicted by the tagging spectrometer. Thus, the raw QDC values can be converted into energies in units of MeV using the linear relation seen in Eq. 2.4.

$$E = ky + E_0 \tag{2.4}$$

where
E = photon energy in MeV
k = slope of the linear fit (*p1* in Fig. 2.19)
y = deposited energy in detector in QDC channels
E_0 = photon energy in MeV corresponding to QDC channel 0 (*p0* in Fig. 2.19)

Eq. 2.4, along with the fit parameters obtained, are used in two calculations, illustrated in Fig. 2.20. The energy calibration is used to obtain a difference between the photon energy determined based on the focal-plane calibrations and the photon energy determined based upon the energy deposited in the NaI detector. If the calibration were perfect, the detector response negligible, and the beam of infinitesimal dimensions, the difference would be zero when the detector is at the inbeam position.

The procedure illustrated in Fig. 2.20 is repeated for all events during a run. The calculated difference for each event is histogrammed in a total spectrum known as the *energy-difference spectrum*. An example of such a spectrum is seen in Fig. 2.21.

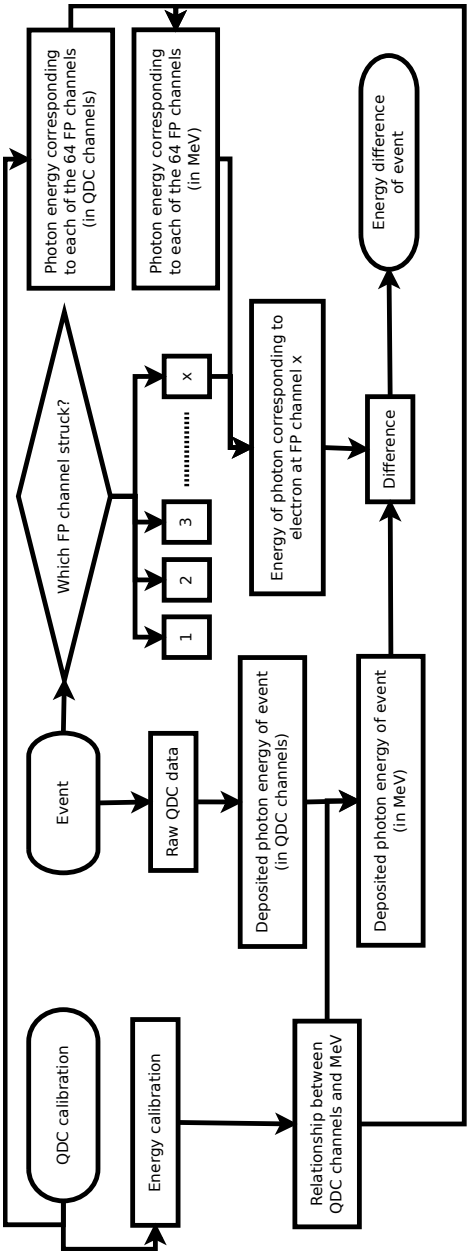

Figure 2.20: Overview of steps resulting in the energy-difference spectrum.

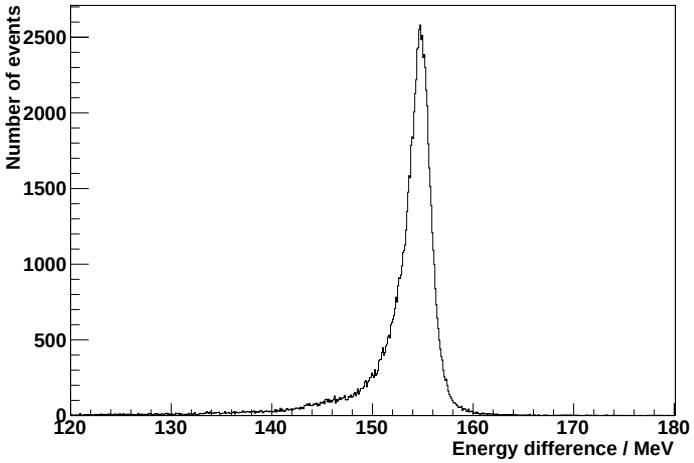

Figure 2.21: Difference in energy deposited between what is expected from the focal-plane calibrations and the calibration of the total gain-matched spectrum. This calibration leads to a peak value centered at 155 MeV as the calculation has been offset by 155 MeV for clarity.

Chapter 3

Results

In this chapter, results of the timing and energy calibrations for BUNI, CATS and DIANA, as well as the timing calibration for the Pb-glass detector, are presented. The data analysed comes from both the June 2011 and April 2012 run periods.

3.1 Pb-glass

The Pb-glass detector is used for tagging-efficiency measurements, and also provides good TDC offset-calibration data.

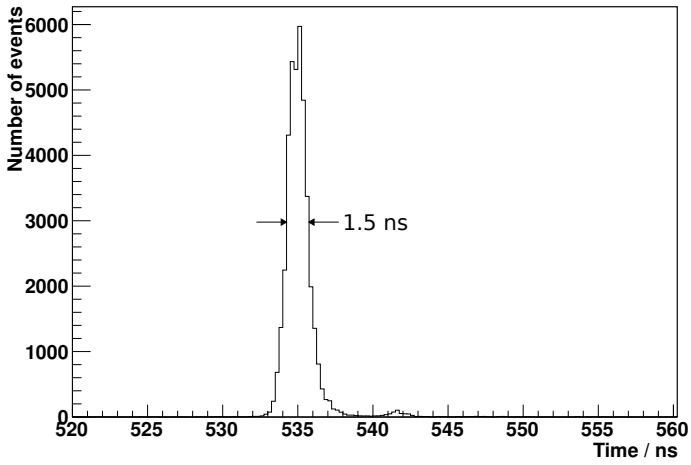

Figure 3.1: Result of the single-hit TDC calibration using Pb-glass run data. The arrows illustrate the peak FWHM of 1.5 ns.

Figure 3.1 shows the single-hit TDC calibration performed with the lead glass data. The peak FWHM is 1.5 ns. Figure 3.2 shows the multi-hit TDC calibration performed with the lead glass data. The peak FWHM is 1.5 ns.

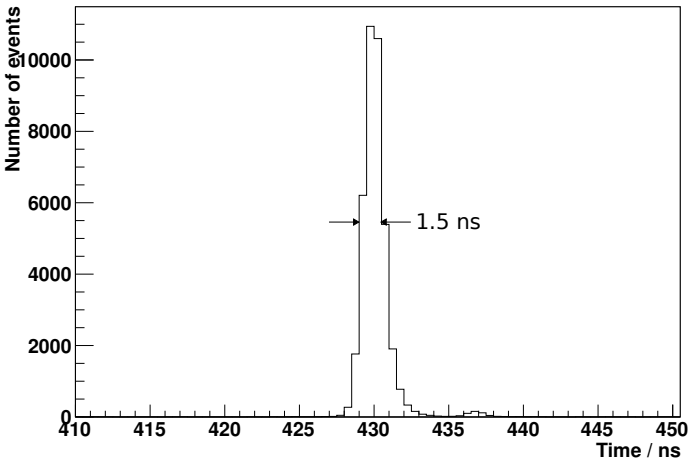

Figure 3.2: Result of the multi-hit TDC calibration using Pb-glass run data. The arrows illustrate the peak FWHM of 1.5 ns.

3.2 BUNI

3.2.1 TDC offset calibration

Fig. 3.3 shows the single-hit TDC calibration performed with the BUNI data. The peak FWHM is 1.3 ns.

The multi-hit TDC calibration shown in Fig. 3.4 has also been performed for the BUNI inbeam data. The calibrated multi-hit TDC peak has a FWHM of 1.5 ns.

3.2.2 QDC calibration

After performing the QDC calibration discussed in Sec. 2.2, a set of energy peak positions (each corresponding to one of the focal-plane channels) was obtained. If the photon energy corresponding to an electron hit in a certain channel has been calculated, an energy calibration can be performed. As in Sec. 2.2.4, the calculated photon energy is plotted against the measured energy deposition. To this, a straight line is fitted.

Using the fit parameters, the energy deposition value in units of QDC channels can be converted into energy units (MeV). This may be done for each

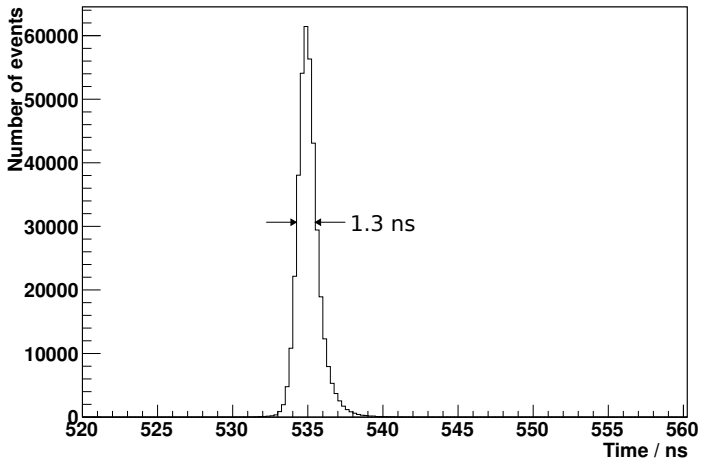

Figure 3.3: Result of the single-hit TDC calibration using BUNI run data. The arrows illustrate the peak FWHM of 1.3 ns.

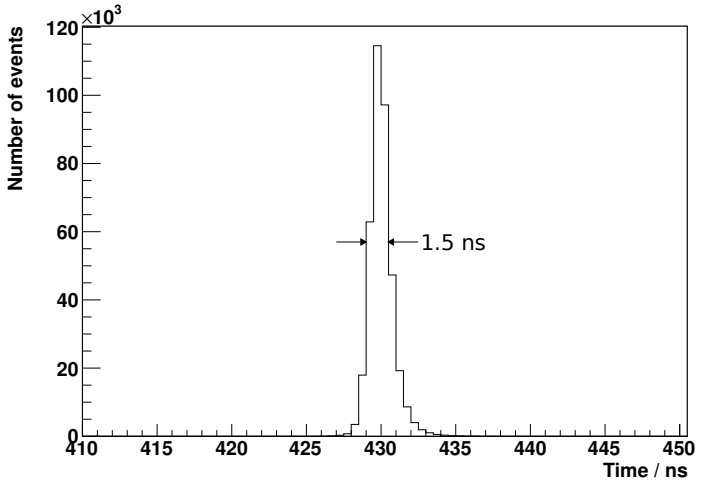

Figure 3.4: Result of the multi-hit TDC calibration using BUNI run data. The arrows illustrate the peak FWHM of 1.5 ns.

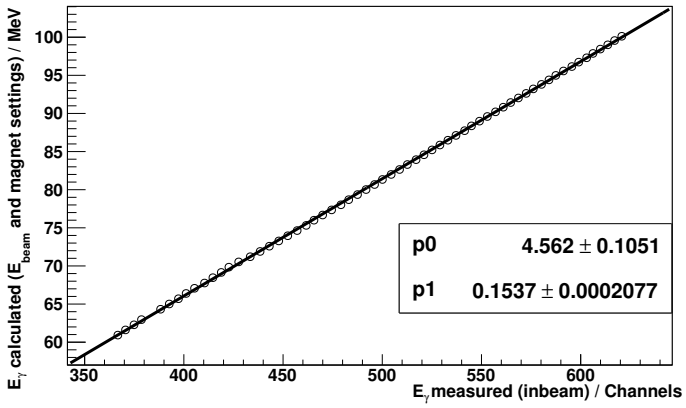

Figure 3.5: Channel-to-energy calibration data and fit for BUNI. The fit parameters are included in the figure. *p0* is the offset and *p1* is the slope of the fit.

focal-plane channel and the QDC data. When taking the difference between the two for each event and then summing over all events, the peak in Fig. 3.6 is obtained. The FWHM of the energy-difference peak in Fig. 3.6 is 2.0 MeV. The peak is arbitrarily positioned at 155 MeV.

3.3 CATS

3.3.1 TDC offset calibration

Fig. 3.7 shows the single-hit TDC calibration performed with the CATS data. The peak FWHM is 2.0 ns.

The multi-hit TDC calibration shown in Fig. 3.8 has also been performed for the CATS inbeam data. The calibrated multi-hit TDC peak has a FWHM of 2.0 ns.

3.3.2 QDC calibration

After performing the QDC calibration discussed in Sec. 2.2, a set of energy peak positions (each corresponding to one of the focal-plane channels) was obtained. If the photon energy corresponding to an electron hit in a certain channel has been calculated, an energy calibration can be performed. As in Sec. 2.2.4, the calculated photon energy is plotted against the measured energy deposition. To this, a straight line is fitted.

Using the fit parameters, the energy deposition value in units of QDC channels can be converted into energy units (MeV). This may be done for each

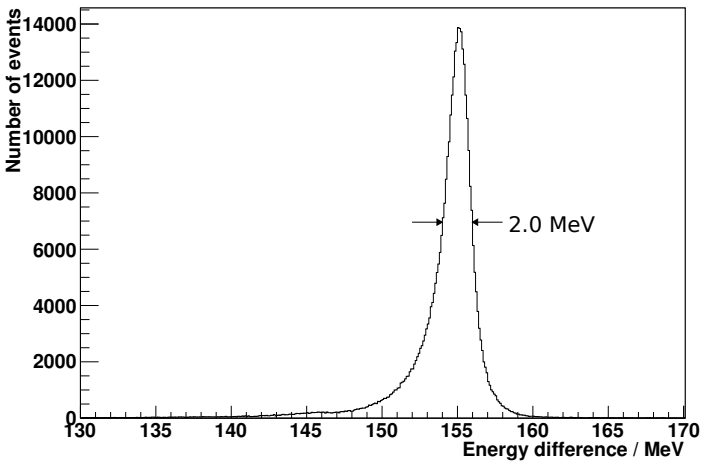

Figure 3.6: Energy calibration peak for BUNI, showing the difference between QDC data and calibration data. The arrows illustrate the peak FWHM of 2.0 MeV.

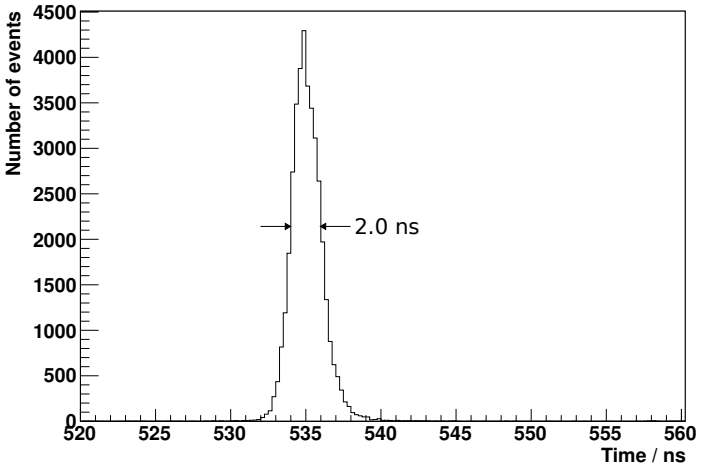

Figure 3.7: Result of the single-hit TDC calibration using CATS run data. The arrows illustrate peak FWHM of 2.0 ns.

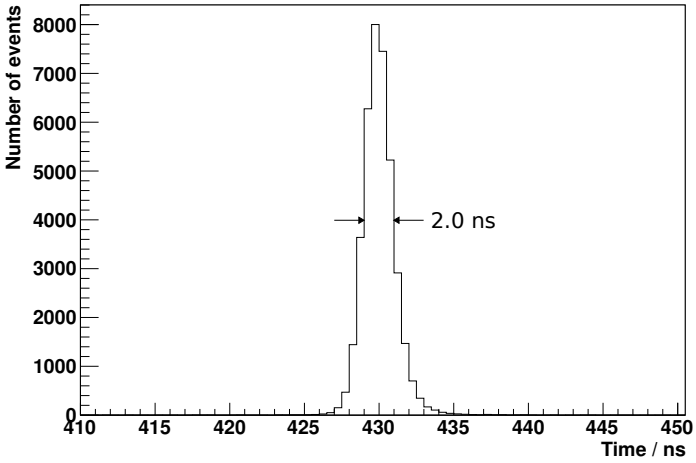

Figure 3.8: Result of the multi-hit TDC calibration using CATS run data. The arrows illustrate the peak FWHM of 2.0 ns.

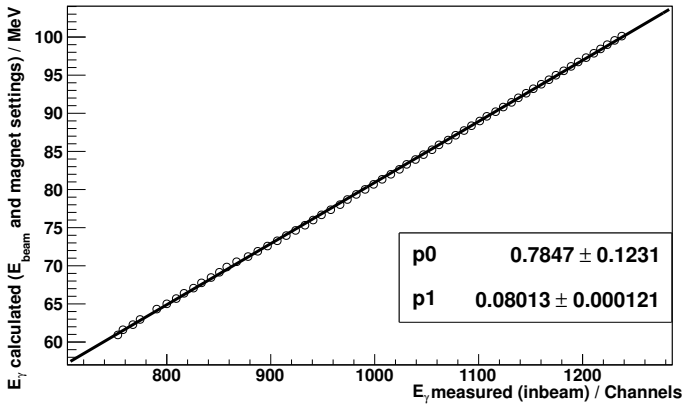

Figure 3.9: Channel-to-energy calibration data and fit for CATS. The fit parameters are included in the figure. *p0* is the offset and *p1* is the slope of the fit.

focal-plane channel and the QDC data. When taking the difference between the two for each event and then summing over all events, the peak in Fig. 3.10 is obtained. The FWHM of the energy-difference peak in Fig. 3.10 is 2.0 MeV. The peak is arbitrarily positioned at 155 MeV.

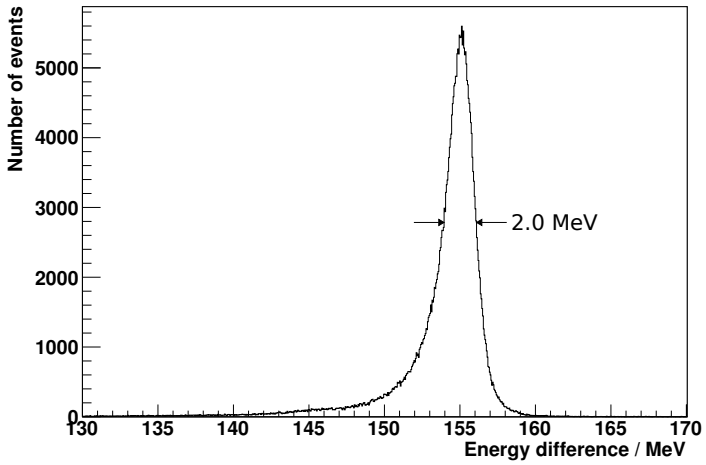

Figure 3.10: Energy calibration peak for CATS, showing the difference between QDC data and calibration data. The arrows illustrate the peak FWHM of 2.0 MeV.

3.4 DIANA

3.4.1 TDC offset calibration

Fig. 3.11 shows the single-hit TDC calibration performed with the DIANA data. The peak FWHM is 1.8 ns.

The multi-hit TDC calibration shown in Fig. 3.12 has also been performed for the DIANA inbeam data. The calibrated multi-hit TDC peak has a FWHM of 2.0 ns.

3.4.2 QDC calibration

After performing the QDC calibration discussed in Sec. 2.2, a set of energy peak positions (each corresponding to one of the focal-plane channels) was obtained. If the photon energy corresponding to an electron hit in a certain channel has been calculated, an energy calibration can be performed. As in Sec. 2.2.4, the calculated photon energy is plotted against the measured energy deposition. To this, a straight line is fitted.

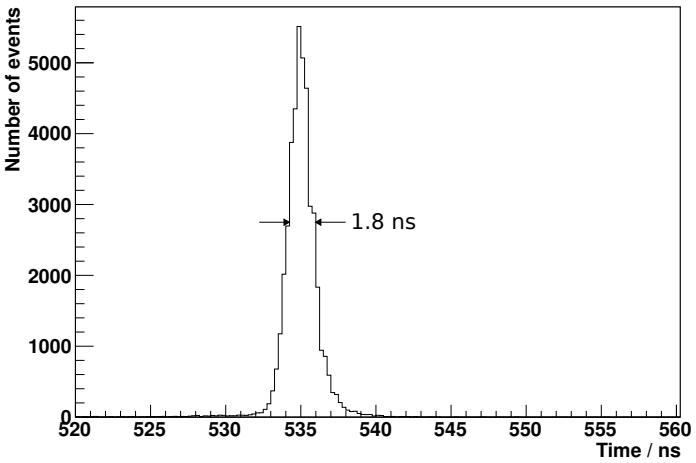

Figure 3.11: Result of the single-hit TDC calibration using DIANA run data. The arrows illustrate the peak FWHM of 1.8 ns.

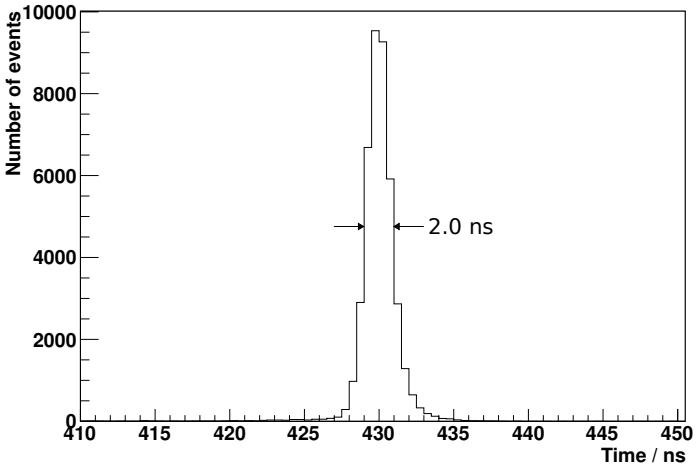

Figure 3.12: Result of the multi-hit TDC calibration using DIANA run data. The arrows illustrate the peak FWHM of 2.0 ns.

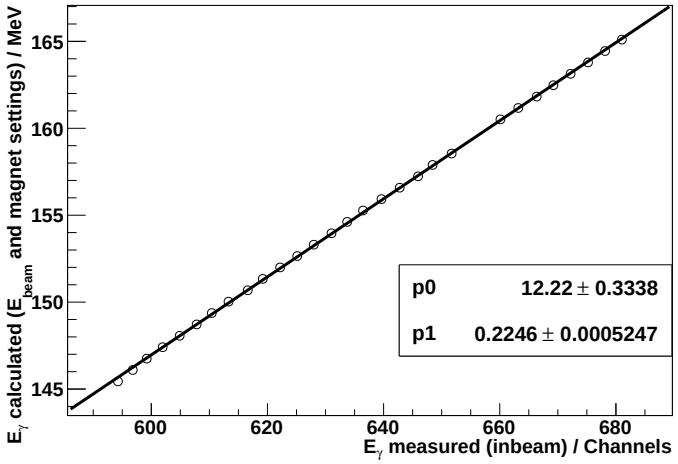

Figure 3.13: Channel-to-energy calibration data and fit for DIANA. The fit parameters are included in the figure. *p0* is the offset and *p1* is the slope of the fit. The reason for the relatively large gap between data points around 160 MeV is because the corresponding focal-plane channel was broken during the run analysed.

Using the fit parameters, the energy deposition value in units of QDC channels can be converted into energy units (MeV). This may be done for each focal-plane channel and the QDC data. When taking the difference between the two for each event and then summing over all events, the peak in Fig. 3.14 is obtained.

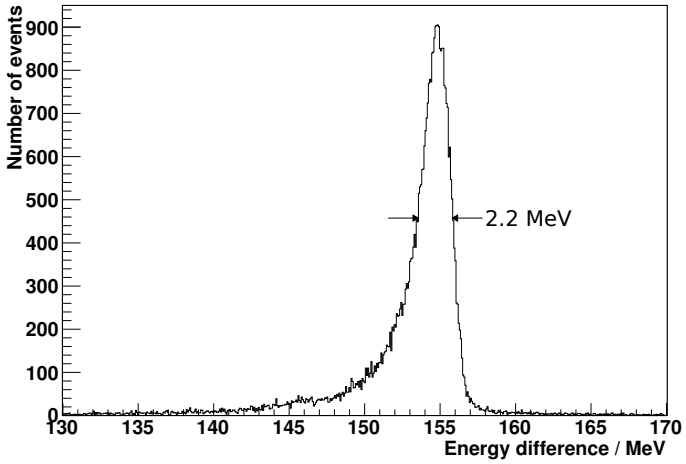

Figure 3.14: Energy calibration peak for DIANA, showing the difference between QDC data and calibration data. The arrows illustrate the peak FWHM of 2.2 MeV.

The FWHM of the energy-difference peak in Fig. 3.14 is 2.2 MeV. The peak is arbitrarily positioned at 155 MeV.

3.5 Summary of results

Table 3.1 presents a summary of the absolute timing resolutions obtained for the four detectors during this analysis. These results are consistent with the recent work of Myers [6].

Table 3.1: Timing offset calibration results

	Single-hit FWHM / ns	Multi-hit FWHM / ns
Pb-glass	1.5	1.5
BUNI	1.3	1.5
CATS	2.0	2.0
DIANA	1.8	2.0

Table 3.2 presents a summary of the absolute energy resolutions obtained for the three large NaI(Tl) detectors during this analysis. These results are consistent with the recent work of Myers [6].

Table 3.2: Energy calibration results

	Core FWHM / MeV	Core and quad/ segment FWHM / MeV
BUNI	3.0	2.0
CATS	4.0	2.0
DIANA	2.2	-

Closing Comment

It is clear from the result presented in this thesis that the detectors have been calibrated. These calibrations may now be used for further in-depth physics analysis of the data collected with these detectors during the run periods in question.

References

[1] "MAX-lab homepage." http://www.maxlab.lu.se/maxlab/about/index.html Page accessed February 3, 2012.

[2] "MAX-lab homepage." http://www.maxlab.lu.se/maxlab/about/max_injector.html Page accessed February 3, 2012.

[3] M. Litwack, "Max-lab May09 Tagging-Efficiency Measurement." Bachelor's Thesis, 2010.

[4] M. Karlsson, *Two-body Photodisintegration of* ^{3}*He*. PhD thesis, Lund University, 2005.

[5] "MAX-lab homepage." https://www.maxlab.lu.se/node/1129 Page accessed August 20, 2012.

[6] L. S. Myers, *Deuteron Compton scattering below pion threshold*. PhD thesis, University of Illinois at Urbana-Champaign, 2010.

[7] "MAX-lab homepage." https://www.maxlab.lu.se/node/1128 Page accessed August 20, 2012.

[8] "MAX-lab homepage." https://www.maxlab.lu.se/node/1127 Page accessed August 20, 2012.

[9] "MAX-lab homepage." https://www.maxlab.lu.se/node/1126 Page accessed August 27, 2012.

[10] "Wikipedia - Particle shower." http://en.wikipedia.org/wiki/Particle_shower Page accessed August 21, 2012.

[11] M. Karlsson, "FYSC01 laboratory instruction, Gamma spectroscopy," 2001. Lund University.

[12] "Wikipedia - Cherenkov radiation." http://en.wikipedia.org/wiki/Cherenkov_radiation Page accessed August 15, 2012.

[13] "Wikipedia - Photomultiplier." http://en.wikipedia.org/wiki/Photomultiplier Page accessed March 22, 2012.

Appendix A

Contribution of the Author

Table A.1 presents a week-by-week summary of the contribution of the author to this project.

Table A.1: Week-by-week project summary

Week	Activity
3	Background reading
4	Background reading
5	Background reading
6	Learning analysis tools
7	Learning analysis tools
8	Learning analysis tools
9	Analysing 2011 data
10	Analysing 2011 data
11	Analysing 2011 data
12	Analysing 2011 data
13	Analysing 2011 data
15	Preparing April experiments
16	April experiments
17	April experiments
18	Analysing April data
19	Analysing April data
20	Analysing April data
21	Analysing April data
22	Analysing April data
23	Writing of thesis
32	Writing of thesis
33	Writing of thesis
34	Writing of thesis

During the execution of this project, the author of this thesis

- learned the required tools for the analysis: C++ and ROOT.
- performed an inbeam analysis on both old (2011) and new (2012) data sets.
- helped people from the University of Glasgow with the experimental setup.
  - Moving the detectors.
  - Repairing the inbeam monitor in the experimental 'cave'.
  - Controlling and labeling cables using a multimeter.
  - Checking signals in the DAQ rooms using an oscilloscope.
  - Setup of the Pb-glass detector before tagging-efficiency runs.
- took data-acquisition shifts during the April experiment.
- described the inbeam analysis to American IRES[1] students during the summer of 2012.

[1] *International Research Experiences for Students*, a placement program for American universities in which the photonuclear group at MAX-lab participates.

Outlook

The calibrations presented in this thesis may be used in the full analysis of data acquired during the respective experimental run periods (June and September 2011 and April 2012). Also, the calibration procedure of the detectors discussed is the same for other run periods as well. Therefore, the same analysis steps will be valid for future analyses of experiments where these detectors are employed. A complete description of the analysis tools, as well as a step-by-step guide to the inbeam analysis, is available in App. D.

Personal reflection

During the past eight months, I have been involved in the work described in this thesis. When starting the project, I had no previous experience of the analysis tools I were to use, and I expected to be performing the inbeam analysis of data taken during 2011. However, I had the possibility of taking part in an experiment in April 2012, thereby getting new data to analyse. I think this period was perhaps the most valuable during the project - not only because of the hands-on experience of being a part of such an experiment, but also to compare the experiment and analysis parts of such a project. While the experiment and data acquisition only went on for a few weeks, the analysis took longer to complete.

However, I really appreciated being able to go into the inbeam analysis in detail, especially as I had the opportunity to use the calibration results in a full scattering analysis (although this was not a part of the actual thesis work) and see the importance of a successful inbeam calibration. Regarding the fact that I had not used the analysis tools (neither C++ nor ROOT) before, I found that my previous programming experiences helped. Also, getting results in every calibration step made it possible to see my progress through the project.

All in all, this project has provided me with valuable research experience which I am certain will be useful in my future studies.

Markus Preston
5 September 2012

Appendix B

Photon-detector components

B.1 Scintillations versus the Čerenkov effect

The photon-detection method varies between the Pb-glass detector and the NaI(Tl) detectors. The NaI(Tl) detectors are scintillators while the Pb-glass detector exploits the Čerenkov effect.

B.1.1 Scintillations

Although scintillators exist in many forms, inorganic thallium-activated sodium-iodide crystals were employed in this work.

The principle behind scintillation in a NaI(Tl) crystal is that an incoming high-energy photon creates a free electron or an electron/positron pair in the crystal through one of the processes illustrated in Fig. B.1 - the Photoelectric effect, Compton Scattering or Pair Production.

Since the atoms bound in the crystal lattice have a much higher mass than an electron and/or positron, the latter will receive approximately all of the incident-photon energy. In the case of pair production, which is the dominating process at the energies at MAX-lab, one electron and one positron are created. The resulting electron and positron will be highly energetic, and will in turn result in further highly energetic photons, electrons, and positrons by the processes described above. A large EGS shower will result. The freed electrons or the electron-positron pairs will travel through the crystal, and while doing so will deposit energy.

The deposition of energy in the crystal by the EGS shower will result in bound atomic electrons in the valence band of the scintillator atoms being excited into the conduction band. An electron in the conduction band will eventually re-combine with a vacancy in the valence band, emitting a photon with an energy corresponding to the energy of the crystal band gap. In order to

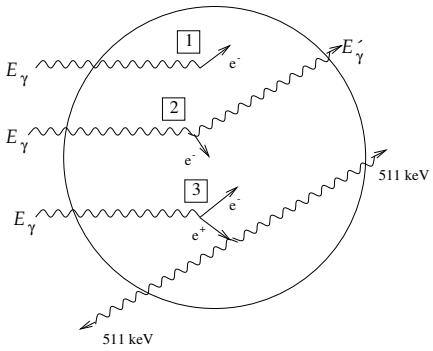

Figure B.1: The three possible interaction processes between incident high-energy photons and the scintillation crystal. 1: Photoelectric effect, 2: Compton scattering, 3: Pair production. Figure from Ref. [11].

increase the efficiency and to avoid de-excitation resulting in the emission of a photon with the same energy as the absorbed photon, the crystal is activated with thallium. Adding thallium atoms to the lattice introduces new energy levels that fall within the bandgap of the unactivated NaI crystal. Thus, de-excitations to these levels will result in photons with lower energies, which are in the near-visible or visible wavelength ranges.

The entire process of interactions within the crystal will thus result in a number of scintillation photons, that are characterized by the fact that they have a longer wavelength than the originally incident photon. The total number of scintillation photons produced will be proportional to the energy of the original photon.

B.1.2 Čerenkov effect

The movement of a charged particle through the medium causes a local perturbation of the electromagnetic field in the medium. This causes the movement of bound electrons, and a polarization of the atoms in which they are bound. In an insulator, the restoration to the equilibrium state of the atom results in the emission of a photon. If the velocity of the particle passing through the material is low, such emitted photons will interfere destructively with each other. However, if the material refractive index n is such that the particle velocity is higher than the phase velocity of light in the same material, the photons will interfere constructively with each other. This is seen as a flash of light, so-called Čerenkov radiation. This light pulse is emitted at an angle θ determined by the refractive index of the material and the particle velocity, see Fig. B.2.

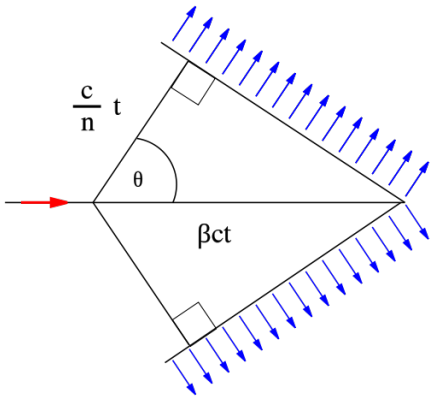

Figure B.2: Geometry of the emission of Čerenkov radiation. Figure from Ref. [12].

B.2 Photomultiplier tubes

To convert the scintillation-light pulse into a measurable current pulse, a photomultiplier tube is used.

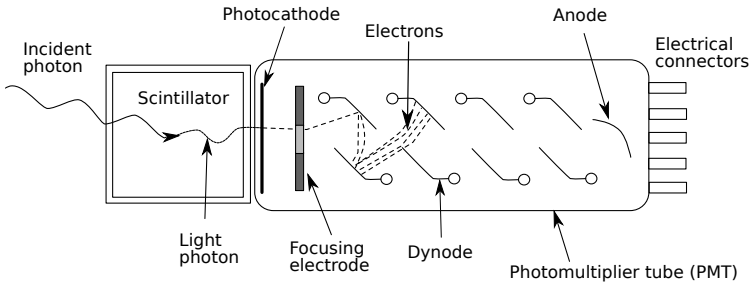

Figure B.3: Schematic view of a scintillator attached to a photomultiplier tube. Shown in the figure is the detection of a single scintillation photon. Figure from Ref. [13].

As shown in Fig. B.3, the scintillation photons strike a photocathode at one end of the PMT. Via the Photoelectric Effect, an electron is emitted from the photocathode. The electron is then accelerated towards the focusing electrode.

After the focusing electrode, a number of dynodes are placed, as seen in the figure. Each dynode has a voltage applied across it. Thus, when the electron passes the focusing electrode, it will be accelerated towards the first dynode. The dynodes are coated with a material from which it is easy to liberate electrons.

When the electron hits the dynode, more electrons are emitted, which together with the original electron are accelerated towards the second dynode. This process is repeated at all dynodes. When the electrons reach the anode, the last 'stage' of the photomultiplier tube, a measureable current pulse has been produced.

Since the number of scintillation photons is proportional to the energy of the original photon incident on the scintillator, so is the amplitude and integral of the current pulse at the anode.

Appendix C

Electronics

C.1 Time-to-Digital Converter

A time-to-digital converter (TDC) is an electronic device that is used to determine the time elapsed between two electric signals - the 'start' and the 'stop'. It consists of a high-frequency oscillator, for which the number of oscillations between a start signal and a stop signal are counted. Thus, its output is an integer number of oscillator counts, which is a digitalized measure of the time between the start and stop.

Two different types of TDCs are used in this work: *single-hit* and *multi-hit*. When single-hit TDC is used, only one start/stop can be processed. Thus, if a start signal is received, only a single stop signal may be produced. On the other hand, a multi-hit TDC is able to process up to four[1] different stop signals corresponding to a single start.

C.2 Charge-to-Digital Converter

A charge-to-digital converter (QDC) is used to integrate the analog current signal from the PMT. When a trigger is generated, a gate signal is sent to the QDC. The length of the gate signal specifies the time over which the analog signal should be integrated. As shown in Fig. C.1, the integral over time of the current at the PMT anode is the total charge in the pulse and is proportional to the energy deposited in the detector.

C.3 Scaler

When an electron is detected at any of the focal-plane channels, a logic signal is sent to a scaler. The scaler simply counts the number of pulses incident upon

[1] Programmable

Figure C.1: Integration of the analog current detected in the photon detector, as performed by the QDC. The gate signal specifies T_1 and T_2. Figure from Ref. [3].

it. Scalers are inherently fast and efficient devices. They accept inhibit pulses to prevent them from registering counts.

C.4 Discriminator

A leading-edge discriminator is a device that looks for analog signals from a detector which are stronger than a fixed level. In the case that the input signal has an amplitude that is greater than the threshold, a logic signal is output. In this manner, a logic one is output if the signal is higher than the threshold, and a logic zero is output if it is lower than the threshold. The width of the logic signal is controlled by the user.

Appendix D

Inbeam calibration guides

D.1 BUNI inbeam calibration

Initialization

Open the `/BuniAnalyzer` directory. Open `Makefile`, and edit it so that the correct file is compiled (this is done by commenting/uncommenting appropriate lines that begin with OFFLINE). Open `inbeam.cxx` and specify the input .root file in the array *DATAFILE*, and the output rootfile in *output*. Open `Inbeam.C` and specify the input file to be the same as the output file of `inbeam.cxx`. Open `find_mh_offsets.C` and do the same thing.

Some important points regarding the datafiles used in the analysis:

- For the focal-plane time calibration, either the BUNI singles trigger or the Pb-glass trigger data must be used.
- For all other calibrations, use the focal-plane OR trigger data.

`inbeam.cxx` is compiled by running `make` in the terminal. ROOT is started by running `root -l` in the terminal. This gives the ROOT prompt, from which scripts (.C files) and the TBrowser can be run.

Before doing the calibrations, the following array initializations must be made:

inbeam.cxx	
offset	[0, 0, 0,..., 0]
mhtdc_offset	[0, 0, 0,..., 0]
ped	[0, 0, 0,..., 0]
b_core	[0, 0, 0,..., 0]
b_energy	[0, 0, 0,..., 0]
bcalib	[0, 1, 1,..., 1]
Inbeam.C	
ped	[0, 0, 0,..., 0]

Focal-plane TDC calibration

Single-hit TDCs

Open `Inbeam.C` in a text editor. Uncomment the code under routine 1 (Self-timing peak position fit for BUNI), and comment all other routines.

Compile `inbeam.cxx`.

Start ROOT and run `Inbeam.C` by typing `.X Inbeam.C` at the ROOT prompt. A Gaussian distribution will be fitted to the *b_tof_raw_[0-63]* spectra. The location of the distribution peak is extracted, thereby obtaining the different channel offsets of the focal-plane single-hit TDC spectra. The offset values are displayed in the terminal.

Enter the values from the terminal window into the array *offset[]* in `inbeam.cxx`. Remake `inbeam.cxx`, and run it by typing `./inbeam` at the terminal prompt. Run TBrowser by typing `new TBrowser` at the ROOT prompt, and locate the *b_T* spectrum in the output file. *b_T* contains the aligned and calibrated focal-plane single-hit TDC coincidence peak for all focal-plane channels. If the FWHM of the peak is about 2 ns, this step worked! Comment out routine 1 in `Inbeam.C`.

Multi-hit TDCs

Compile `inbeam.cxx`.

Start ROOT and run `find_mh_offsets.C` by typing `.X find_mh_offsets.C` at the ROOT prompt. A Gaussian distribution will be fitted to the *b_mh_T_[0-63]* spectra. The locations of the peaks are fitted, thereby obtaining the different channel offsets of the focal-plane multi-hit TDC spectra. The offset values are displayed in the terminal.

Enter the values from the terminal window into the array *mhtdc_offset[]* in `inbeam.cxx`. Remake `inbeam.cxx`, and run it by typing `./inbeam` at the terminal prompt. Run TBrowser by typing `new TBrowser` in the ROOT prompt, and locate the *b_mh_Sum* spectrum in the output file. *b_mh_Sum* contains the aligned and calibrated focal-plane multi-hit TDC coincidence peak for all focal-plane channels. If the FWHM of the peak is about 2 ns, this step worked!

Core and quad PMT pedestals

Uncomment routine 2 (core+quad pedestal fit for BUNI) in `Inbeam.C`, and comment all other routines.

Start ROOT and run `Inbeam.C`. Routine 2 fits a Gaussian distribution to the pedestal spectra *b_ped_[0-10]*, and extracts the channel offset for each PMT in BUNI. BUNI is not all core, but consists of a core surrounded by four 'quads'. Thus, seven of the PMTs belong to the core, while each quad has several PMTs that are daisy-chained into a single signal. The offset values from the fits are output in the terminal window.

Copy the values from the terminal window. Paste them into the *ped[]* array in `Inbeam.C` and as the last 11 elements of the *ped[]* array in `inbeam.cxx`. Note

that element zero of *ped[]* in `inbeam.cxx` should always be zero, due to the configuration of the electronics.

Remake `inbeam.cxx`, and run it with `./inbeam`. Comment out routine 2 in `Inbeam.C`.

Core PMT gain-matching

Uncomment routine 3 (core PMT spectra fit for BUNI) in `Inbeam.C`, and comment all other routines.

Start ROOT and run `Inbeam.C`. The *b_core_[0-6]fp_[0-63]* spectra, which contain the gain peaks for the BUNI core PMTs on a focal-plane channel-by-channel basis, are fitted in order to extract the position of these peaks. Since the peak position for a given focal-plane channel depends on the electron energy corresponding to that channel, the peaks will be shifted with respect to each other. Seven equally spaced focal-plane channels are selected, and the seven peak positions for each of these channels are determined. This results in a two-dimensional array, containing 7x7 elements.

The peak position of each PMT relative to that of the central core PMT is then determined. This is done by first calculating the ratio between an element in the first row of the 2d array (corresponding to one of seven focal-plane channels and the central PMT) and an element in the same column (corresponding to the same focal-plane channel) and another row (corresponding to another core PMT). This procedure is repeated for the whole array, giving 7x7 ratios (the ratios in row 0 are all 1.000, since the ratios are in a sense the positions relative to the central core PMT, which is row zero in the array). For each PMT, the elements are averaged, and a 1d array is created, containing seven values. These values give a relation between the core PMT gain peak positions. As such, if any of the 6 non-central core PMT spectra is multiplied with its corresponding average ratio, it is shifted so that its peak position is the same as for the central core PMT.

The resulting ratios are output to the terminal. Enter these values as the seven first non-zero values in the *bcalib[]* array of `inbeam.cxx`, while leaving the last four elements at their initialization values (which is 1). Note that the first element in *bcalib[]* should always be 0, due to the configuration of the electronics. Remake `inbeam.cxx`, and run it with `./inbeam`. 64 gain-matched spectra are created as *b_coresum_fp_[0-63]*.

Comment out routine 3 in `Inbeam.C`.

Core PMT summed spectra peak positions

Above, relations between the positions of the gain peaks for all core PMTs were calculated. Now, the sum of the spectra for all core PMTs for each focal-plane channel will be calibrated, so that there is one gain peak corresponding to all core events.

Uncomment routine 4 (core spectrum fit for BUNI for each focal-plane channel) in `Inbeam.C`, and comment all other routines.

Start ROOT and run `Inbeam.C`. The gain-matched peaks that also have been summed for all core PMTs to form the spectra *b_coresum_fp_[0-63]* are fitted in order to extract the positions of these peaks. The resulting peak positions (one for each focal-plane channel) are displayed in the terminal.

Copy these values from the terminal, and paste them into the array *b_core[]* in `inbeam.cxx`.

Compile `inbeam.cxx`, and run it with `./inbeam`. This creates a gain-matched spectrum containing the sum of all events in the BUNI core PMTs. Recall that BUNI is not all core, so that further steps remain.

Comment out routine 4 in `Inbeam.C`.

Relating the quad and core signals

Since BUNI consists of both a core and four quads, there is a possibility that a photon entering the detector gives rise to a particle shower too big to be contained in the core. This leads to a signal leakage to the quads, which has to be added to the signal detected in the core. The different quads have different gains however, making it necessary to first scale them, before adding them back into the core signal.

Open ROOT and run `ShieldCalib.C`.

The spectra *b_corevseg_[0-3]* are opened. They contain the number of photons detected as a function of the energy deposited in the core and the energy deposited in the selected quad (there is one spectrum for each quad). That is, the *b_corevseg_[0-3]* spectra are originally two-dimensional histograms. They are divided into slices based on the energy in the quad, and these slices are then projected onto new one-dimensional histograms. To these projections, Landau distributions are fitted. When this is done for all slices for a specific quad, there is a relation between the slice fit position and the core energy. These peak positions are then plotted as a function of the quad slice QDC channel, and a straight line is fitted to these results. This is done for all four quads, giving four line slopes. These slope values are displayed in the terminal. Copy them into the last four elements of the *bcalib[]* array in `inbeam.cxx`.

Compile `inbeam.cxx`, and run it with `./inbeam`. Now the quad addback correction has been added to the spectra.

Core and quad PMT summed spectra peak positions

Above, relations between the positions of the gain peaks for all core and quad PMTs have been calculated. Now, the sum of the spectra for all core and quad PMTs for each focal-plane channel will be calibrated, so that there is one gain peak corresponding to all core and quad events.

Uncomment routine 5 (coresegsum spectrum fit for BUNI for each focal-plane channel) in `Inbeam.C`, and comment all other routines.

Start ROOT and run `Inbeam.C`. The gain-matched peaks that also have been summed for all core and quad PMTs to form the spectra *b_coresegsum_fp_[0-63]*

are fitted in order to extract the positions of these peaks. The resulting peak positions (one for each focal-plane channel) are displayed in the terminal.

Copy these values from the terminal, and paste them into the array *b_energy[]* in `inbeam.cxx`.

Compile `inbeam.cxx`, and run it with `./inbeam`. This creates a gain-matched spectrum containing the sum of all events in the BUNI core and quad PMTs.

Comment out routine 5 in `Inbeam.C`.

Channel-to-energy calibration

Open `Fit.C`. The *y[]* array contains the energies in MeV from bremsstrahlung photons corresponding to each of the focal-plane channels. This is therefore the photon energy predicted from the photon-tagging process, which can be compared to the photon energy detected in BUNI. After the calibrations in the above steps, the detected energy (in channels) for each of the focal-plane channels is stored in the *b_energy[]* array in `inbeam.cxx`.

Copy the desired elements from this array into the *energy[]* array in `Fit.C`. Note that there might be broken focal-plane channels, making it necessary to remove the corresponding array elements from both *y[]* and *energy[]*.

Start ROOT and run `Fit.C`. A straight line is fitted to the values, giving a calibration curve between photon energy in channels and MeV. The first-degree polynomial coefficients (the y-intercept and the line slope) are displayed both in the plot and in the terminal. The values in the terminal should be used. Copy the two coefficients into the equations for the variable *energy* and the array *b_energy[]* in `inbeam.cxx`.

Compile `inbeam.cxx` and run it with `./inbeam`. Run ROOT and open TBrowser. Examine the *b_E* spectrum, which contains the difference between the expected energy in the *coresegsum* spectrum from focal-plane calibrations and the actual energy in *coresegsum*. A peak with a FWHM of about 2 MeV means that the calibrations worked.

D.2 CATS inbeam calibration

Initialization

Open the `/CatsAnalyzer` directory. Open `Makefile`, and edit it so that the correct file is compiled (this is done by commenting/uncommenting appropriate lines that begin with OFFLINE). Open `inbeam.cxx` and specify the input .root file in the array *DATAFILE*, and the output rootfile in *output*. Open `Inbeam.C` and specify the input file to be the same as the output file of `inbeam.cxx`. Open `find_mh_offsets.C` and do the same thing.

Some important points regarding the datafiles used in the analysis:

- For the focal-plane time calibration, either the CATS singles trigger or the Pb-glass trigger data must be used.

- For all other calibrations, use the focal-plane OR trigger data.

`inbeam.cxx` is compiled by running `make` in the terminal. ROOT is started by running `root -l` in the terminal. This gives the ROOT prompt, from which scripts (.C files) and the TBrowser can be run.

Before doing the calibrations, the following array initializations must be made:

inbeam.cxx	
offset	[0, 0, 0,..., 0]
mhtdc_offset	[0, 0, 0,..., 0]
ped	[0, 0, 0,..., 0]
c_core	[0, 0, 0,..., 0]
c_energy	[0, 0, 0,..., 0]
ccalib	[1, 1, 1,..., 1]
Inbeam.C	
ped	[0, 0, 0,..., 0]

Focal-plane TDC calibration

Single-hit TDCs

Open `Inbeam.C` in a text editor. Uncomment the code under routine 1 (Self-timing peak position fit for CATS), and comment all other routines.

Compile `inbeam.cxx`.

Start ROOT and run `Inbeam.C` by typing `.X Inbeam.C` at the ROOT prompt. A Gaussian distribution will be fitted to the *c_tof_raw_[0-63]* spectra. The location of the distribution peak is extracted, thereby obtaining the different channel offsets of the focal-plane single-hit TDC spectra. The offset values are displayed in the terminal.

Enter the values from the terminal window into the array *offset[]* in `inbeam.cxx`. Remake `inbeam.cxx`, and run it by typing `./inbeam` at the terminal prompt. Run TBrowser by typing `new TBrowser` at the ROOT prompt, and locate the c_T spectrum in the output file. c_T contains the aligned and calibrated focal-plane single-hit TDC coincidence peak for all focal-plane channels. If the FWHM of the peak is about 2 ns, this step worked! Comment out routine 1 in `Inbeam.C`.

Multi-hit TDCs

Compile `inbeam.cxx`.

Start ROOT and run `find_mh_offsets.C` by typing `.X find_mh_offsets.C` at the ROOT prompt. A Gaussian distribution will be fitted to the *c_mh_T_[0-63]* spectra. The locations of the peaks are fitted, thereby obtaining the different channel offsets of the focal-plane multi-hit TDC spectra. The offset values are displayed in the terminal.

Enter the values from the terminal window into the array *mhtdc_offset[]* in `inbeam.cxx`. Remake `inbeam.cxx`, and run it by typing `./inbeam` at the terminal prompt. Run TBrowser by typing `new TBrowser` at the ROOT prompt, and locate the *c_mh_Sum* spectrum in the output file. *c_mh_Sum* contains the aligned and calibrated focal-plane multi-hit TDC coincidence peak for all focal-plane channels. If the FWHM of the peak is about 2 ns, this step worked!

Core and segment PMT pedestals

Uncomment routine 2 (core+segment pedestal fit for CATS) in `Inbeam.C`, and comment all other routines.

Start ROOT and run `Inbeam.C`. Routine 2 fits a Gaussian distribution to the pedestal spectra *c_ped_[0-12]*, and extracts the channel offset for each PMT in CATS. CATS is not all core, but consists of a core surrounded by six segments. Thus, seven of the PMTs belong to the core, while each segment has several PMTs that are daisy-chained into a single signal. The offset values from the fits are output in the terminal window.

Copy the values from the terminal window. Paste them into the *ped[]* array in `Inbeam.C` and the *ped[]* array in `inbeam.cxx`.

Remake `inbeam.cxx`, and run it with `./inbeam`. Comment out routine 2 in `Inbeam.C`.

Core PMT gain-matching

Uncomment routine 3 (core PMT spectra fit for CATS) in `Inbeam.C`, and comment all other routines.

Start ROOT and run `Inbeam.C`. The *c_core_[0-6]fp_[0-63]* spectra, which contain the gain peaks for the CATS core PMTs on a focal-plane channel-by-channel basis, are fitted in order to extract the position of these peaks. Since the peak position for a given focal-plane channel depends on the electron energy corresponding to that channel, the peaks will be shifted with respect to each other. Seven equally spaced focal-plane channels are selected, and the seven peak positions for each of these channels are determined. This results in a two-dimensional array, containing 7x7 elements.

The peak position of each PMT relative to that of the central core PMT is then determined. This is done by first calculating the ratio between an element in the first row of the 2d array (corresponding to one of seven focal-plane channels and the central PMT) and an element in the same column (corresponding to the same focal-plane channel) and another row (corresponding to another core PMT). This procedure is repeated for the whole array, giving 7x7 ratios (the ratios in row 0 are all 1.000, since the ratios are in a sense the positions relative to the central core PMT, which is row zero in the array). For each PMT, the elements are averaged, and a 1d array is created, containing seven values. These values give a relation between the core PMT gain peak positions. As such, if any of the 6 non-central core PMT spectra is multiplied with its

corresponding average ratio, it is shifted so that its peak position is the same as for the central core PMT.

The resulting ratios are output to the terminal. Enter these values as the seven first values in the *ccalib[]* array of `inbeam.cxx`, while leaving the last six elements at their initialization values (which is 1). Remake `inbeam.cxx`, and run it with `./inbeam`. 64 gain-matched spectra are created as *c_coresum_fp_[0-63]*.

Comment out routine 3 in `Inbeam.C`.

Core PMT summed spectra peak positions

Above, relations between the positions of the gain peaks for all core PMTs were calculated. Now, the sum of the spectra for all core PMTs for each focal-plane channel will be calibrated, so that there is one gain peak corresponding to all core events.

Uncomment routine 4 (core spectrum fit for CATS for each focal-plane channel) in `Inbeam.C`, and comment all other routines.

Start ROOT and run `Inbeam.C`. The gain-matched peaks that also have been summed for all core PMTs to form the spectra *c_coresum_fp_[0-63]* are fitted in order to extract the positions of these peaks. The resulting peak positions (one for each focal-plane channel) are displayed in the terminal.

Copy these values from the terminal, and paste them into the array *c_core[]* in `inbeam.cxx`.

Compile `inbeam.cxx`, and run it with `./inbeam`. This creates a gain-matched spectrum containing the sum of all events in the CATS core PMTs. Recall that CATS is not all core, so that further steps remain.

Comment out routine 4 in `Inbeam.C`.

Relating the segment and core signals

Since CATS consists of both a core and six segments, there is a possibility that a photon entering the detector gives rise to a particle shower too big to be contained in the core. This leads to a signal leakage to the segments, which has to be added to the signal detected in the core. The different segments have different gains however, making it necessary to first scale them, before adding them back into the core signal.

Open ROOT and run `ShieldCalib.C`.

The spectra *c_corevseg_[0-5]* are opened. They contain the number of photons detected as a function of the energy deposited in the core and the energy deposited in the selected segment (there is one spectrum for each segment). That is, the *c_corevseg_[0-5]* spectra are originally two-dimensional histograms. They are divided into slices based on the energy in the segment, and these slices are then projected onto new one-dimensional histograms. To these projections, Landau distributions are fitted. When this is done for all slices for a specific segment, there is a relation between the slice fit position and the core energy. These peak positions are then plotted as a function of the segment slice QDC

channel, and a straight line is fitted to these results. This is done for all six segments, giving six line slopes. These slope values are displayed in the terminal. Copy them into the last six elements of the *ccalib[]* array in `inbeam.cxx`.

Compile `inbeam.cxx`, and run it with `./inbeam`. Now the segment addback correction has been added to the spectra.

Core and segment PMT summed spectra peak positions

Above, relations between the positions of the gain peaks for all core and segment PMTs have been calculated. Now, the sum of the spectra for all core and segment PMTs for each focal-plane channel will be calibrated, so that there is one gain peak corresponding to all core and segment events.

Uncomment routine 5 (coresegsum spectrum fit for CATS for each focal-plane channel) in `Inbeam.C`, and comment all other routines.

Start ROOT and run `Inbeam.C`. The gain-matched peaks that also have been summed for all core and segment PMTs to form the spectra *c_coresegsum_fp_[0-63]* are fitted in order to extract the positions of these peaks. The resulting peak positions (one for each focal-plane channel) are displayed in the terminal.

Copy these values from the terminal, and paste them into the array *c_energy[]* in `inbeam.cxx`.

Compile `inbeam.cxx`, and run it with `./inbeam`. This creates a gain-matched spectrum containing the sum of all events in the CATS core and segment PMTs.

Comment out routine 5 in `Inbeam.C`.

Channel-to-energy calibration

Open `Fit.C`. The *y[]* array contains the energies in MeV from bremsstrahlung photons corresponding to each of the focal-plane channels. This is therefore the photon energy predicted from the photon-tagging process, which can be compared to the photon energy detected in CATS. After the calibrations in the above steps, the detected energy (in channels) for each of the focal-plane channels is stored in the *c_energy[]* array in `inbeam.cxx`.

Copy the desired elements from this array into the *energy[]* array in `Fit.C`. Note that there might be broken focal-plane channels, making it necessary to remove the corresponding array elements from both *y[]* and *energy[]*.

Start ROOT and run `Fit.C`. A straight line is fitted to the values, giving a calibration curve between photon energy in channels and MeV. The first-degree polynomial coefficients (the y-intercept and the line slope) are displayed both in the plot and in the terminal. The values in the terminal should be used. Copy the two coefficients into the equations for the variable *energy* and the array *c_energy[]* in `inbeam.cxx`.

Compile `inbeam.cxx` and run it with `./inbeam`. Run ROOT and open TBrowser. Examine the *c_E* spectrum, which contains the difference between the expected energy in the *coresegsum* spectrum from focal-plane calibrations and the actual energy in *coresegsum*. A peak with a FWHM of about 2 MeV means that the calibrations worked.

D.3 DIANA inbeam calibration

Initialization

Open the `/DianaAnalyzer` directory. Open `Makefile`, and edit it so that the correct file is compiled (this is done by commenting/uncommenting appropriate lines that begin with OFFLINE). Open `inbeam.cxx` and specify the input .root file in the array *DATAFILE*, and the output rootfile in *output*. Open `Inbeam.C` and specify the input file to be the same as the output file of `inbeam.cxx`. Open `find_mh_offsets.C` and do the same thing.

Some important points regarding the datafiles used in the analysis:

- For the focal-plane time calibration, either the DIANA singles trigger or the Pb-glass trigger data must be used.
- For all other calibrations, use the DIANA singles or DIANA singles+FP OR data.
- Do not use the FP OR trigger data.

`inbeam.cxx` is compiled by running `make` in the terminal. ROOT is started by running `root -l` in the terminal. This gives the ROOT prompt, from which scripts (.C files) and the TBrowser can be run.

Before doing the calibrations, the following array initializations must be made:

inbeam.cxx	
offset	[0, 0, 0,..., 0]
mhtdc_offset	[0, 0, 0,..., 0]
ped	[0, 0, 0,..., 0]
d_energy	[0, 0, 0,..., 0]
dcalib	[1, 1, 1,..., 1]
Inbeam.C	
ped	[0, 0, 0,..., 0]

Focal-plane TDC calibration

Single-hit TDCs

Open `Inbeam.C` in a text editor. Uncomment the code under routine 1 (Self-timing peak position fit for DIANA), and comment all other routines.

Compile `inbeam.cxx`.

Start ROOT and run `Inbeam.C` by typing `.X Inbeam.C` at the ROOT prompt. A Gaussian distribution will be fitted to the *d_tof_raw_[0-63]* spectra. The location of the distribution peak is extracted, thereby obtaining the different channel offsets of the focal-plane single-hit TDC spectra. The offset values are displayed in the terminal.

Enter the values from the terminal window into the array *offset[]* in `inbeam.cxx`. Remake `inbeam.cxx`, and run it by typing `./inbeam` at the terminal prompt.

Run TBrowser by typing `new TBrowser` at the ROOT prompt, and locate the *d_T* spectrum in the output file. *d_T* contains the aligned and calibrated focal-plane single-hit TDC coincidence peak for all focal-plane channels. If the FWHM of the peak is about 2 ns, this step worked! Comment out routine 1 in `Inbeam.C`.

Multi-hit TDCs

Compile `inbeam.cxx`.

Start ROOT and run `find_mh_offsets.C` by typing `.X find_mh_offsets.C` at the ROOT prompt. A Gaussian distribution will be fitted to the *d_mh_T_[0-63]* spectra. The locations of the peaks are fitted, thereby obtaining the different channel offsets of the focal-plane multi-hit TDC spectra. The offset values are displayed in the terminal.

Enter the values from the terminal window into the array *mhtdc_offset[]* in `inbeam.cxx`. Remake `inbeam.cxx`, and run it by typing `./inbeam` at the terminal prompt. Run TBrowser by typing `new TBrowser` in the ROOT prompt, and locate the *d_mh_Sum* spectrum in the output file. *d_mh_Sum* contains the aligned and calibrated focal-plane multi-hit TDC coincidence peak for all focal-plane channels. If the FWHM of the peak is about 2 ns, this step worked!

Core PMT pedestals

Uncomment routine 2 (core PMT pedestal fit for DIANA) in `Inbeam.C`, and comment all other routines.

Start ROOT and run `Inbeam.C`. Routine 2 fits a Gaussian distribution to the pedestal spectra *d_ped_[0-18]*, and extracts the channel offset for each PMT in the DIANA core. These values are output in the terminal window. Note that the first of these values, corresponding to the pedestal offset for the central PMT, is not correct for DIANA. This has to be obtained from elsewhere.

Copy the values (except for the first one, for the reasons given above) from the terminal window. Paste them into the *ped[]* array in `Inbeam.C` and the *ped[]* array in `inbeam.cxx`.

Remake `inbeam.cxx`, and run it with `./inbeam`. Comment out routine 2 in `Inbeam.C`.

Core PMT gain-matching

Uncomment routine 3 (core PMT spectra fit for DIANA) in `Inbeam.C`, and comment all other routines.

Start ROOT and run `Inbeam.C`. The *d_core_[0-18]fp_[0-63]* spectra, which contain the gain peaks for the DIANA core PMTs on a focal-plane channel-by-channel basis, are fitted in order to extract the position of these peaks. Since the peak position for a given focal-plane channel depends on the electron energy corresponding to that channel, the peaks will be shifted with respect to each other. Seven equally spaced focal-plane channels are selected, and the

19 peak positions for each of these channels are determined. This results in a two-dimensional array, containing 19x7 elements.

The peak position of each PMT relative to that of the central core PMT is then determined. This is done by first calculating the ratio between an element in the first row of the 2d array (corresponding to one of seven focal-plane channels and the central PMT) and an element in the same column (corresponding to the same focal-plane channel) and another row (corresponding to another PMT). This procedure is repeated for the whole array, giving 19x7 ratios (the ratios in row 0 are all 1.000, since the ratios are in a sense the positions relative to the central PMT, which is row zero in the array). For each PMT, the elements are averaged, and a 1d array is created, containing 19 values. These values give a relation between the PMT gain peak positions. As such, if any of the 18 non-central PMT spectra is multiplied with its corresponding average ratio, it is shifted so that its peak position is the same as for the central PMT.

The resulting ratios are output to the terminal. Copy these values into the *dcalib[]* array of `inbeam.cxx`. Remake `inbeam.cxx`, and run it with `./inbeam`. 64 gain-matched spectra are created as *d_coresum_fp_[0-63]*.

Comment out routine 3 in `Inbeam.C`.

Core PMT summed spectra peak positions

Above, relations between the positions of the gain peaks for all PMTs were calculated. Now, the sum of the spectra for all PMTs for each focal-plane channel will be calibrated, so that there is one gain peak corresponding to all events.

Uncomment routine 4 (core spectrum fit for DIANA for each focal-plane channel) in `Inbeam.C`, and comment all other routines.

Start ROOT and run `Inbeam.C`. The gain-matched peaks that also have been summed for all PMTs to form the spectra *d_coresum_fp_[0-63]* are fitted in order to extract the positions of these peaks. The resulting peak positions (one for each focal-plane channel) are displayed in the terminal.

Copy these values from the terminal, and paste them into the array *d_energy[]* in `inbeam.cxx`.

Comment out routine 4 in `Inbeam.C`.

Channel-to-energy calibration

Open `Fit.C`. The *y[]* array contains the energies in MeV from bremsstrahlung photons corresponding to each of the focal-plane channels. This is therefore the photon energy predicted from the photon-tagging process, which can be compared to the photon energy detected in DIANA. After the calibrations in the above steps, the detected energy (in channels) for each of the focal-plane channels is stored in the *d_energy[]* array in `inbeam.cxx`.

Copy the desired elements from this array into the *energy[]* array in `Fit.C`. Note that there might be broken focal-plane channels, making it necessary to remove the corresponding array elements from both *y[]* and *energy[]*.

Start ROOT and run `Fit.C`. A straight line is fitted to the values, giving a calibration curve between photon energy in channels and MeV. The first-degree polynomial coefficients (the y-intercept and the line slope) are displayed both in the plot and in the terminal. The values in the terminal should be used. Copy the two coefficients into the equations for the variable *energy* and the array *d_energy[]* in `inbeam.cxx`.

Compile `inbeam.cxx` and run it with `./inbeam`. Run ROOT and open TBrowser. Examine the *d_E* spectrum, which contains the difference between the expected energy in the *coresum* spectrum from focal-plane calibrations and the actual energy in *coresum*. A peak with a FWHM of about 2 MeV means that the calibrations worked.